Oncogenic RAS signaling suppresses ferroptosis via transcriptional upregulation of GCH1

Jonathan K. M. Lim[1*], Frauke Stölting[1#], Tal Levy[2,3#], Leonie Thewes[4], Daniel Picard[1,5,6] Sofya Tishina[7,8], Hai-Feng Zhang[9,10], Oksana Lewandowska[1,11], Tobias Reiff[11], Marc Remke[1,5,6], Johannes Brägelmann[7,12,13], Filippo Beleggia[7,12,14], Carsten Berndt[4], Silvia von Karstedt[7,8,13], Guido Reifenberger[1,6], Barak Rotblat[2,3], Gabriel Leprivier[1*]

[1]*Institute of Neuropathology, University Hospital Düsseldorf and Medical Faculty, Heinrich Heine University, Düsseldorf, Germany*

[2]*Department of Life Sciences, Faculty of Natural Sciences, Ben-Gurion University of the Negev, Beer-Sheva, Israel*

[3]*The National Institute for Biotechnology in the Negev, Ben-Gurion University of the Negev, Beer-Sheva, Israel*

[4]*Department of Neurology, University Hospital Düsseldorf and Medical Faculty, Heinrich-Heine University Düsseldorf, Düsseldorf, Germany*

[5]*Department of Pediatric Oncology, Hematology, and Clinical Immunology, University Hospital Düsseldorf and Medical Faculty, Heinrich Heine University, Düsseldorf, Germany*

[6]*German Cancer Consortium (DKTK) partner site Essen/Düsseldorf, Düsseldorf, Germany*

[7]*Department of Translational Genomics, University Hospital Cologne and Faculty of Medicine, University of Cologne, Cologne, Germany*

[8]*CECAD Cluster of Excellence, University of Cologne, Cologne, Germany*

[9]*Department of Pathology and Laboratory Medicine, University of British Columbia, Vancouver, BC, Canada*

[10]*Department of Molecular Oncology, BC Cancer Agency, Vancouver, BC, Canada*

[11]*Institute of Genetics, Heinrich-Heine-University, Düsseldorf, Germany*

[12]*Mildred Scheel School of Oncology Aachen Bonn Cologne Düsseldorf (MSSO ABCD), Faculty of Medicine and University Hospital Cologne, University of Cologne, Cologne, Germany*

[13]*Center for Molecular Medicine Cologne (CMMC), Faculty of Medicine and University Hospital Cologne, University of Cologne, Cologne, Germany*

[14]*Department I of Internal Medicine, Faculty of Medicine and University Hospital Cologne, University of Cologne, Cologne, Germany*

[*]Correspondence: jonathan.lim@med.uni-duesseldorf.de, gabriel.leprivier@med.uni-duesseldorf.de

[#]Equal contribution

Abstract

Ferroptosis is an iron-dependent form of regulated cell death arising from excessive lipid peroxidation. While seminal work described that oncogenic RAS transformation drives synthetic lethal vulnerability to archetypal ferroptosis inducers including erastin (eradicator of RAS and ST-expressing cells) and RSL3 (Ras selective lethal 3), more recent work suggest that oncogenic RAS signaling may confer ferroptosis resistance. Thus, the impact of oncogenic RAS on the cellular response to ferroptosis is still unclear. Here, we provide unifying evidence across multiple cellular models that oncogenic RAS signaling suppresses ferroptosis. Using integrated proteo- and transcriptomic analyses, we uncovered that

oncogenic RAS signaling upregulates the ferroptosis suppressor GTP cyclohydrolase I (GCH1) via transcriptional induction by the transcription factor ETS1 downstream of the RAS-MAPK signaling cascade. Targeted repression of Gch1 or of the tetrahydrobiopterin (BH4) synthesis pathway, which is mediated by GCH1, was sufficient to sensitize oncogenic RAS transformed cells to ferroptosis in 2D and 3D cell models, highlighting a mechanism through which RAS promotes resistance to ferroptosis induction. Furthermore, we found that GCH1 expression is clinically relevant and correlates with RAS signaling activation in human cancers. Overall, this study redefines oncogenic RAS signaling to be a ferroptosis suppressor, and identifies GCH1 as a mediator of this effect and a potential vulnerability for targeting RAS driven cancers.

Introduction

Ferroptosis is an iron-dependent, non-apoptotic form of cell death resulting from the excessive accumulation of lipid hydroperoxides. Cellular defenses against ferroptosis are mediated by the combined action of the cystine/glutamate antiporter xCT, which dictates the rates of glutathione (GSH) biosynthesis by importing cystine, as well as the GSH-dependent selenoenzyme glutathione peroxidase 4 (GPX4), which directly detoxifies lipid hydroperoxides (1–4). Independent of the xCT-GPX4 axis, other major regulators of ferroptosis include ferroptosis suppressor protein 1 (FSP1), which mediates ubiquinol (CoQH2) recycling, and GTP cyclohydrolase 1 (GCH1), which mediates tetrahydrobiopterin (BH4) synthesis, both of which are lipophilic radical-trapping antioxidants with the propensity to reduce toxic lipid hydroperoxides (5–9). Ferroptosis has been implicated in cancer and is proposed to act as a barrier against tumorigenesis. Indeed, the tumor suppressors p53 and BAP1 have been individually linked to ferroptosis induction through their ability to repress the expression of *SLC7A11* (the gene encoding xCT) (10, 11). Intriguingly, ferroptosis was initially described in synthetic lethal screens used to identify compounds that preferentially kill mutant RAS^{G12V} transformed cells but not normal isogenic counterparts – termed RAS-selective lethal (RSL) compounds, which include erastin (xCT inhibitor) and RSL3 (GPX4 inhibitor) (12–14). These initial studies suggest that oncogenic RAS sensitizes cells to ferroptosis, which was supported by some studies using newly-discovered ferroptosis inducers (FINs)(3, 15).

RAS is a small GTPase encoded by the *HRAS*, *KRAS*, and *NRAS* proto-oncogenes (16–18). Physiologically, RAS is responsible for transmitting growth factors signals from receptor tyrosine kinases through to the activation of the prototypical RAF-MEK-ERK and PI3K-AKT pathways, which promote proliferation and survival, respectively (17, 18). *RAS* genes are frequently mutated in human cancer, particularly in pancreatic, colorectal, and lung adenocarcinomas (18). Upon mutation, RAS acquires oncogenic properties that mediate tumor initiation and maintenance. Furthermore, oncogenic RAS confers resistance to apoptosis through multiple signaling cascades, rendering it difficult to target RAS-mutant tumors (19–21). Therefore, exploiting ferroptosis induction as a means to circumvent such resistance represents an attractive alternative approach to treating RAS-mutant cancers.

Nonetheless, the impact of oncogenic RAS on ferroptosis is still unclear. Despite the initial discovery of ferroptosis as an oncogenic RAS-selective lethality in the cellular systems mentioned, previous work by us and others demonstrated that oncogenic RAS in fact enhances intracellular anti-oxidant capacity. In particular, we demonstrated that oncogenic RAS signaling transcriptionally upregulates *SCL7A11* to promote glutathione biosynthesis and confer resistance to oxidative stress (22). Furthermore, we recently reported that oncogenic RAS induces FSP1 transcription to protect cells against RSL3-induced ferroptosis (23). Thus, the *bona fide* role of oncogenic RAS in modulating the response to ferroptosis needs to be clarified, as this holds significant future ramifications for the clinical application of FINs as a cancer therapy.

Here, we provide substantial evidence across multiple cellular models that oncogenic RAS expression suppresses ferroptosis induction by multiple classes of FINs, strongly supporting that oncogenic RAS signaling mediates the protection of cells, rather than their sensitization

to ferroptosis induction. Transcriptome and proteomic profiling further reveal that among various ferroptosis modulators, *GCH1* expression is highly upregulated upon KRAS^{G12V} transformation. Indeed, we provide strong evidence that *GCH1* transcription is under the regulation of the transcription factor ETS1 downstream of the RAS-driven RAF-MEK-ERK pathway. Functionally, we uncovered that GCH1 and BH4 synthesis contributes to oncogenic KRAS^{G12V}-mediated ferroptosis resistance and reduction of lipid peroxidation (LP) in vitro and in vivo. This has clinical relevance as we report that *GCH1* expression is increased in RAS mutant tumors. Collectively, these findings offer 1) a renewed perspective for the role of oncogenic RAS as a predictor of ferroptosis resistance, 2) the mechanism by which this occurs, and 3) the translational potential of inhibiting GCH1/BH4 as a novel strategy for the sensitization of RAS mutant tumors to ferroptosis.

Results

Oncogenic RAS signaling activation confers resistance to ferroptosis

The role of oncogenic RAS in modulating cellular susceptibility to ferroptosis is still controversial. To provide unifying evidence as to the impact of oncogenic RAS on ferroptosis, we sought to interrogate the response of multiple isogenic cellular RAS systems to different classes of ferroptosis inducers (FINs). First, we found that mouse NIH 3T3 fibroblasts transformed with mutant KRAS^{G12V} (NIH 3T3 KRAS^{G12V}) were completely resistant to the class I FINs erastin and sulfasalazine (SSZ), class II FINs ML162 and ML210, and class IV FIN FINO2, while non-transformed counterparts NIH 3T3 MSCV showed varying levels of cell death following a 16-hour treatment with each of these compounds (Fig. 1A and S1A). This is consistent with our previous findings that mouse embryonic fibroblasts display enhanced resistance to the class II FIN RSL3 following endogenous level expression of oncogenic KRAS (23). Co-treatment with the ferroptosis-selective antioxidant ferrostatin-1 (Fer-1) abolished cell death induced in non-transformed fibroblasts by the different FINs, confirming the induction of ferroptosis (Fig. 1A and Fig. S1A). Strikingly, NIH 3T3 KRAS^{G12V} were completely resistant even when exposed to high concentrations of erastin (up to 20 μM), while non-transformed cells were susceptible across a range of erastin treatment (Fig. S1A). Second, we confirmed these initial observations using a derivative of a widely-utilized mutant RAS overexpression system, namely human BJ fibroblasts immortalized with the catalytic subunit of human telomerase (hTERT), SV40 large T and small T antigen (LT and ST respectively) and transformed by ectopic expression of oncogenic HRAS^{G12V} (BJ-hTERT/LT/ST/HRAS^{G12V}, also known as BJeLR cells) (2, 3, 24). These models previously led to the identification of RSL3 and erastin as selective lethal agents against cells expressing both mutant RAS and small T antigen (ST) (12–14). To determine the impact of mutant RAS in these models, but independently of ST, we subjected BJ-hTERT/LT/HRAS^{G12V} and the corresponding isogenic BJ-hTERT/LT control cells to FINs treatment. Interestingly, BJ-hTERT/LT/HRAS^{G12V} showed enhanced resistance to RSL3, ML162, ML210 and erastin, as compared to BJ-TERT/LT (Fig. 1B), in contrast to previous findings obtained with BJeLR compared to BJ-hTERT (12–14). While these results further support that oncogenic RAS confers resistance against ferroptosis induction, they also highlight the contribution of ST to ferroptosis sensitivity (12). In agreement with increased resistance to multiple FINs and our previously reported data, BJ-hTERT/LT/HRAS^{G12V} cells expressed higher levels of SLC7A11 and FSP1 than BJ-hTERT/LT (Fig. S1, B and C) (22, 23). Third, to extend the validity of our findings in human cell lines, we assessed the impact of KRAS depletion on susceptibility to ferroptosis, using shRNA-mediated knockdown of KRAS in mutant KRAS^{G12V}-expressing human pancreatic adenocarcinoma cell line CFPAC1. Notably, KRAS knockdown rendered CFPAC1 cells more sensitive to RSL3-induced cell death, which was again rescued by Fer-1 (Fig. 1C and D).

Finally, to determine the generalizability of oncogenic RAS-mediated resistance to ferroptosis, we leveraged cancer cell line drug sensitivity data from the Cancer Therapeutic Response Portal v2 (CTRPv2), available from Broad Institute's DepMap portal (25, 26). We observed a correlation across over 700 cancer cell lines between *KRAS* mutation and resistance (i.e.,

148 higher median area under the curve [AUC] values) to ML162 (Fig. 1E), while this was not
149 observed for RSL3, ML210, and erastin (Fig. S1, D to F). Given that the RAS pathway can be
150 active even in cancer cells harboring *KRAS wild-type* (*KRAS*^{wt}), due to various genetic events,
151 we analyzed RAS pathway activity in the same dataset using a validated transcriptional
152 signature of 84 genes (RAS84) optimized to capture RAS oncogenic activity (27). Remarkably,
153 we found that higher RAS pathway activation positively correlated with resistance to ML162,
154 RSL3, ML210, and erastin (Fig. 1, F to I). Taken together, these findings provide strong
155 evidence that oncogenic RAS signaling activation functionally protects cells from ferroptosis
156 and correlates with ferroptosis resistance across a large number of cancer cells.

157 **Oncogenic RAS signaling leads to upregulation of GCH1**

158 The fact that RAS pathway activation correlates with ferroptosis resistance across many
159 cancer entities suggests that it may be mediated by additional mechanisms besides FSP1 and
160 xCT upregulation. Therefore, we next sought to identify novel downstream mediators of
161 oncogenic RAS signaling that could protect cells against ferroptosis. To this end, we
162 performed RNA sequencing of NIH 3T3 KRAS^{G12V} and control cells and integrated this data
163 with our previous proteomics analysis performed on the same cell lines (28). These screens
164 identified 2022 transcripts and 448 proteins that were significantly altered following KRAS^{G12V}-
165 expression, among which were 193 overlapping transcripts/proteins (Fig. S2A). Consistent
166 with our prior investigations, transcriptome profiling identified *Slc7a11* and *Aifm2* (encoding
167 Fsp1), but not *Gpx4*, as upregulated by oncogenic RAS signaling (Fig. 2A). Notably, the gene
168 encoding GTP cyclohydrolase I, *Gch1*, was among the most significantly upregulated genes
169 in NIH 3T3 KRAS^{G12V} cells (Fig. 2A). Indeed, among the 193 overlapping transcripts/proteins
170 significantly altered in KRAS^{G12V}-expressing cells, Gch1 represented the 5th most upregulated
171 transcript and 10th most upregulated protein (Table S1). Importantly, GCH1 was recently
172 identified as a suppressor of ferroptosis (7, 8). Indeed, GCH1 is the rate-limiting enzyme in
173 tetrahydrobiopterin (BH4) synthesis, a radical-trapping antioxidant with potent activity against
174 LP (Fig. 2B) (8). For this reason, we decided to focus on the regulation of *GCH1* by oncogenic
175 RAS. The upregulation of *Gch1* in NIH 3T3 KRAS^{G12V} versus control cells was confirmed using
176 qRT-PCR (Fig. 2C), as well as at the protein level using mass spectrometry-based proteomics
177 (Fig. 2D). In agreement, human BJ-hTERT/LT/HRAS^{G12V} cells showed a similar increase in
178 *GCH1* expression relative to BJ-hTERT/LT isogenic counterparts (Fig. 2E). In human cancer
179 cells harboring *KRAS* mutations, including CFPAC1 and non-small cell lung carcinoma cell
180 line H460, shRNA-mediated knockdown of KRAS conversely led to decreases in *GCH1*
181 expression (Fig. 2, F and G and Fig. S2B). Similarly, treatment of mutant KRAS^{G12C}-expressing
182 pancreatic cancer cell line MIA PaCa-2 with the KRAS^{G12C} inhibitor AMG 510 decreased *GCH1*
183 expression (Figure 2H).

184 Additionally, by analyzing expression data of IMR90 human fibroblasts we found elevated
185 *GCH1* expression upon stable expression of HRAS^{G12V}, as compared to control pBabe, but
186 not upon constitutively active AKT1 (Figure 2I) (29). This suggests that *GCH1* might be
187 upregulated downstream of RAS-MAPK signaling but not PI3K-AKT signaling. To further
188 ascertain this, we treated NIH 3T3 KRAS^{G12V} cells with the MEK inhibitor PD184352 or the
189 AKT inhibitor MK-2206 and found that the former but not the latter led to decreased *Gch1*
190 expression, further supporting that the regulation of *GCH1* downstream of oncogenic RAS is
191 mediated by MAPK (RAF-MEK-ERK) signaling (Figure 2J). Moreover, MEK inhibition led to a
192 sustained depletion of *Gch1* expression for up to 72 hours (Fig. S2C). Altogether, the data
193 suggests that oncogenic RAS signaling leads to upregulation of *GCH1* expression in a MAPK-
194 dependent manner.

195 **GCH1 mediates oncogenic RAS-driven ferroptosis resistance**

196 We next investigated the role of GCH1 in mediating ferroptosis suppression downstream of
197 oncogenic RAS signaling. For these studies, we first employed ferroptosis sensitive non-
198 transformed NIH 3T3 cells to determine whether supplementation with BH4, the end product
199 of the biosynthesis pathway downstream of GCH1, could phenocopy ferroptosis resistance

mediated by KRAS-mutant expression in these cells. Strikingly, cells supplemented with BH4, or its oxidized form dihydrobiopterin (BH2), showed near-complete insensitivity to erastin or FINO2, similar to NIH 3T3 KRAS^{G12V} cells (Fig. 3, A and B). While NIH 3T3 MSCV exhibited higher amounts of LP as NIH 3T3 KRAS^{G12V} cells when treated with erastin or FINO2, consistent with the ferroptosis-related phenotypes observed in these cells, the levels of LP were significantly reduced upon supplementation of NIH 3T3 MSCV with BH2 (Fig. 3, C and D). This was not the case with BH4 treatment (Fig. 3, C and D), suggesting a possible difference in the mechanism of ferroptosis protection between BH2 and BH4, or decreased BH4 efficiency since the oxidation of BH4 upon contact with culture medium may yield multiple oxidation products. Furthermore, BH4 or BH2 supplementation abrogated ferroptosis sensitivity of KRAS-knockdown CFPAC1 cells under RSL3 treatment (Fig. 3E), linking mutant KRAS-mediated ferroptosis resistance to the activity of the BH4 synthesis pathway. Finally, to ascertain of the contribution of GCH1 to KRAS^{G12V}-mediated resistance to ferroptosis, we knocked down *Gch1* expression in NIH 3T3 KRAS^{G12V} cells using CRISPR interference (CRISPRi). This was sufficient to restore the sensitivity of NIH 3T3 KRAS^{G12V} to ferroptosis induced by erastin or FINO2 (Fig. 3F and G, Fig. S3A). Taken together, these findings suggest that oncogenic RAS signaling leads to ferroptosis resistance by co-opting GCH1 function.

Targeting the BH4 synthesis pathway sensitizes oncogenic RAS to ferroptosis in vivo

Next, we sought to determine the contribution of GCH1 to oncogenic RAS-mediated tumorigenic potential or the ability of GCH1 inhibition to synergize with ferroptosis induction in vivo. To this end, we first assessed the ability of NIH 3T3 KRAS^{G12V} cells to grow under anchorage-independent conditions following CRISPRi-mediated *Gch1* knockdown using soft agar colony formation assays. While knockdown of *Gch1* expression did not observably decrease colony growth of KRAS-transformed cells under normal conditions, it resulted in significantly decreased tumorigenic potential of these cells under conditions of ferroptosis induction, suggesting that GCH1 inhibition may also synergize with ferroptosis induction in vivo (Fig. 4A and Fig. S3C). Similarly, this effect was observed in KRAS-transformed cells treated with SPRi3, an inhibitor against sepiapterin reductase (SPR), the enzyme mediating the final step of BH4 synthesis (Fig. 2B), under ferroptosis-induced conditions (Fig. 4B). In agreement, SPRi3 treatment synergized with RSL3-mediated ferroptosis induction in reducing the size of pancreatic organoids derived from the LsL-KRAS^{G12D} transgenic mouse model of pancreatic cancer (Fig. 4C) (30).

***GCH1* expression is clinically relevant and correlates with oncogenic RAS activation in human cancers**

It was previously reported that *GCH1* expression contributes to lung cancer, breast cancer, and glioblastoma development and that its overexpression is linked to poor prognosis of glioblastoma patients (31–33). Given the potential of GCH1 inhibition as a therapeutic strategy for the sensitization of RAS driven tumors to ferroptosis induction, we now analyzed the clinical relevance of *GCH1* expression in human cancers harboring KRAS mutation or constitutive RAS signaling activation through analysis of The Cancer Genome Atlas (TCGA) datasets. Notably, a pan-cancer analysis revealed that *GCH1* expression is higher in *KRAS-mutant* (*KRAS^{mut}*) tumors than in *KRAS^{wt}* tumors (Fig. 5A). We then extended the same analysis of *GCH1* expression to several tumor types of which a significant proportion of tumors are known to harbour activating mutations in *KRAS*, namely pancreatic adenocarcinoma (PAAD), colon adenocarcinoma (COAD) and lung adenocarcinoma (LUAD). Such analyses revealed that *GCH1* is overexpressed in PAAD, COAD, and LUAD relative to corresponding non-tumor tissue (Fig. 5, B, C, and D). Further, *GCH1* overexpression was confirmed in two orthogonal PAAD datasets (Fig. S4A and B) (34, 35). Consistent with the above-findings, we observed a positive correlation between *GCH1* levels and RAS signaling activation (based on RAS84 signature) in COAD, but also in several other human cancers including rectal adenocarcinoma (READ), uterine carcinosarcoma (UCS), skin cutaneous melanoma (SKCM), low-grade glioma (LGG), and GBM (Fig. 5E-J). Of note, *GCH1* expression was recently reported to be elevated

in glioblastoma but the mechanisms by which this occurs remains unclear (31). Together with previous reports that genetic alterations in components of the RAS-MAPK cascade are frequently observed in glioblastoma, our evidence suggests that *GCH1* overexpression is associated with oncogenic RAS signaling activation in this tumor type (36). In agreement, over-representation analysis of genes positively co-expressed with *GCH1* in glioblastoma exhibited significant enrichment of genes known to be upregulated upon KRAS activation (Fig. 5K). Moreover, *Gch1* levels are higher in tumors derived from a genetically engineered mouse model of high-grade glioma, constituted from *Nf1*-deletion (which promotes RAS pathway activation), as compared to matched normal tissue (Fig. 5L), but this was not observed in a *c-Myc*-driven mouse model of liver carcinoma (Fig. S4C) (37). Together, our findings reveal the clinical relevance of *GCH1* regulation by the oncogenic RAS pathway in human cancers.

Transcriptional upregulation of *GCH1* by oncogenic RAS signaling is mediated by ETS1

We next sought to determine the mechanism by which oncogenic RAS signaling regulates *GCH1* expression. To this end, we conducted gene set enrichment analysis (GSEA) of genes displaying positive co-expression with *Gch1* from the above RNA sequencing data of NIH 3T3 $KRAS^{G12V}$ and control cells. Notably, genes having at least one binding site for the transcription factor Ets-1 showed significant enrichment, and this gene set was among the top five transcription factor target gene sets showing enrichment (Fig. 6A, Fig. S5A). Given the fact that ETS1 is a known substrate of ERK downstream of the RAS-MAPK signaling pathway, we postulated that the regulation of *GCH1* by oncogenic RAS is mediated by ETS1, which to our knowledge has not been reported (Fig. 6B). In support of this, siRNA-mediated knockdown of *Ets-1* expression in NIH 3T3 $KRAS^{G12V}$ cells significantly decreased *Gch1* expression (Fig. 6C). Similarly, knockdown of *ETS1* expression in H460 cells using two distinct siRNAs led to a decrease in *GCH1* expression (Fig. 6D). Next, to ascertain whether ETS1 controls the induction of *GCH1*, we performed dual-luciferase reporter assays in HEK293T cells using a reporter construct consisting of a transcriptionally active region (TAR) of *GCH1* directly upstream of *Firefly luciferase*. Sequence analysis of this region revealed the presence of three ETS1 binding sites, based on the consensus 5'-GGAA/T-3' (Fig. 6E). While ectopic ETS1 expression was sufficient to activate the TAR of *GCH1* in a dose-dependent manner, mutations in each of three putative ETS1 binding sites within this region abrogated this effect, with concurrent mutations in all three sites having the strongest effect (Fig. 6, F and G). In support of this, chromatin immunoprecipitation (ChIP)-qRT-PCR in NIH 3T3 $KRAS^{G12V}$ cells and ChIP-sequencing analysis of publicly-available UCSC Encode data provided strong evidence that endogenous ETS1 occupies the human and mouse TAR region of *GCH1* (Fig. 6, H and I). Consistent with our functional analyses above, pan-cancer data from the Clinical Proteomic Tumor Analysis Consortium (CPTAC) indicate that *GCH1* expression levels are positively correlated with ETS1 protein expression (Fig. 6J), whereas publicly-available PAAD, COAD, and LUAD datasets similarly show a positive correlation between *GCH1* and *ETS1* mRNA expression (Fig. 6, K to M) (35, 38, 39). Together, these data support that *GCH1* is transcriptionally upregulated by the MEK-ERK-ETS1 pathway downstream of oncogenic RAS.

Discussion

There is a growing interest in the potential of inducing ferroptosis in tumor cells as an anticancer strategy. However, ferroptosis sensitivity varies substantially among cancer cells due to distinct tissue lineages, mutation status of oncogenes or tumor suppressor genes, as well as the acquisition of drug-tolerant or differentiated cell states (3, 10, 40–42). Thus, understanding the mechanisms that contribute to LP and ferroptosis will aid the development of effective approaches to overcome ferroptosis resistance. In this study, we demonstrate that oncogenic activation of RAS signaling, one of the most mutated pathways in cancer, is a major determinant of ferroptosis resistance. Notably, ferroptosis originally emerged as an alternative form of necrosis induced by erastin and RSL3, identified from synthetic lethal compound screens for their selective cytotoxicity towards engineered mutant HRAS-overexpressing cells known as BJeLR cells (12–14). Following these seminal findings, the identification of novel

classes of FINs have often been accompanied by validation in the BJeLR model, over time substantiating a paradigm that oncogenic RAS-transformed cells are ostensibly sensitive to ferroptosis inducers, even though the association between KRAS mutational status and ferroptosis sensitivity could never be confirmed in comprehensive human cancer cell line screens (3, 43). On the contrary, our findings here, together with our previous study suggest rather that oncogenic RAS signaling renders cells resistant to ferroptosis, as demonstrated using multiple functional models (23). One of the models used here, BJ-hTERT/LT/HRAS^{V12} cells, are similar to BJeLR but allowed us to interrogate the effect of mutant RAS independently of ST, which was initially used as an additional transforming factor. Indeed, in the absence of ST, mutant HRAS^{V12} expression led to a paradoxical resistance to FINs suggesting that the presence of ST may confound the contribution of RAS signaling in modulating the sensitivity of cells to ferroptosis. Notably, one of the mechanisms by which ST promotes malignant transformation is by negatively regulating the protein phosphatase 2A (PP2A) family (24). Thus, the mechanisms by which ST or PP2A possibly modulate ferroptosis response warrant further investigation.

It was previously suggested that the expression level of mutant RAS, whether expressed from an endogenous locus or ectopically overexpressed, will have differential effects on ferroptosis sensitivity of the cell, depending ultimately on the net outcome of how cellular processes related to ferroptosis, including metabolism, redox and iron homeostasis, are balanced (23, 44, 45). This could plausibly explain why oncogenic RAS sensitizes cells to ferroptosis in some contexts, while in others protect cells from ferroptosis. However, our previous findings in endogenous KRAS cellular models and current findings in ectopic cellular KRAS and HRAS models, all demonstrably protect cells from FINs. An independent study similarly observed that rhabdomyosarcoma cells were protected against ferroptosis upon ectopic expression of various oncogenic RAS isoforms (46). In support of this, our survey of a large array of cancer cell lines (from the CCLE database) also revealed a significant association between oncogenic RAS signaling activation and ferroptosis resistance. Altogether, our evidence from various contexts are in accordance with a role of oncogenic RAS signaling as a ferroptosis suppressor, and highlights that the accepted view of ferroptosis as a synthetic lethal vulnerability of RAS-driven tumors needs to be revisited.

A major finding of our work is that oncogenic activation of the RAS signaling pathway induces GCH1 transcription to promote ferroptosis suppression. GCH1 is the rate-limiting enzyme in de novo synthesis of cellular BH4, converting GTP to dihydroneopterin phosphate (NH2TP), which is further processed to 6-pyruvoyltetrahydropterin (6-PTP) via 6-pyruvoyltetrahydropterin synthase (PTS), and finally producing BH4 via SPR (47). In turn, BH4 is an essential cofactor for a number of enzymes including nitric oxide synthases (NOSs) and tyrosine hydroxylase, critical for the synthesis of nitric oxide (NO) and dopamine respectively. More recently, BH4 itself was described to be a potent antioxidant with the ability to trap lipid radicals and prevent the propagation of LP chain reaction, as well as to selectively prevent oxidative degradation of polyunsaturated fatty acyl chain-containing phospholipids that drive ferroptosis execution (7, 8). Consistently, we found that *GCH1*-depletion re-sensitized KRAS-mutant cells to ferroptosis induction, while BH4 supplementation potently rescued this effect. In our cellular models, a direct radical-trapping effect of BH4 is likely, but an indirect effect of BH4 from its cofactor role cannot be completely ruled out. Intriguingly, BH4 reduction leads to uncoupling of NOSs, resulting in superoxide generation, which can promote ferroptosis. Conversely, NO, even though considered a radical species, paradoxically has been described to suppress ferroptosis by terminating LP propagation (48). Further, evidence suggest that GCH1 overexpression leads to an accumulation of the antioxidant CoQH2, since BH4 is also a cofactor for phenylalanine to tyrosine conversion, which can generate 4-OH-benzoate, a precursor for CoQH2 synthesis (7). It is therefore conceivable that BH4 generation downstream of oncogenic RAS signaling could also protect cells against ferroptosis via NOS- or CoQH2-dependent mechanisms. Of note, although the enhancement of GCH1-mediated BH4 synthesis is sufficient to suppress ferroptosis, oxidized BH4 (BH2) can also be

regenerated via the function of dihydrofolate reductase (DHFR) (8). Thus, whether DHFR serves a compensatory role for BH4 maintenance under GCH1-depleted conditions, and whether simultaneously targeting BH4 synthesis and DHFR using pharmacological inhibitors may be a viable therapeutic strategy against RAS-driven cancers, is likely to be a subject of future interest.

Interestingly, GCH1 was reported to play a role in promoting tumorigenesis. In particular, GCH1 was shown to facilitate the growth of glioblastoma in vivo, possibly by preserving the redox balance (31). In line with that, Cronin *et al.* recently demonstrated that GCH1 contributes to the development of non-small cell lung cancer NSCLC in a genetically-engineered mouse model driven by KRAS (32). In both studies, whether the pro-tumorigenic function of GCH1 is linked to the control of ferroptosis is unclear. While our data do not show that GCH1 is a determinant of tumorigenicity of KRAS-transformed fibroblasts in vitro and in vivo, this may be due to the lack of contribution from the tumor microenvironment or the absence of a fully functional immune system. Yet, we provide evidence that targeting GCH1 or SPR sensitizes cells to ferroptosis induction in KRAS-driven cancer models in vitro and in tumor organoids. Taken together, while targeting GCH1 alone could be a viable therapeutic strategy to target RAS driven tumors, our findings suggest that combining inhibitors of the BH4 pathway with FINs, such as IKE, may represent a more effective therapeutic approach to target these tumor types. Alternatively, combining RAS pathway inhibitors with FINs may prove to be an attractive therapeutic strategy since we and others have shown that repressing RAS signaling may sensitize cells to FINs, particularly in light of well-documented resistance to RAS inhibitors (49, 50).

In summary, this study uncovers that oncogenic RAS signaling transcriptionally regulates the GCH1-BH4 axis to mediate ferroptosis resistance. Along with our previous work, we thus demonstrate that oncogenic RAS signaling induces an extensive transcriptional program promoting the upregulation of three major arms of ferroptosis defense which also includes the xCT-glutathione axis and the FSP1-CoQH2 axis (22, 23). Consistently, our findings redefine the role of oncogenic RAS signaling to be a ferroptosis suppressor, which may help guide future strategies to maximize the clinical utility of FINs as next-generation therapeutic modalities against refractory and recurrent RAS-mutant tumors.

Materials and Methods

Cell culture

NIH 3T3 cells expressing mutant $KRAS^{G12V}$ and control MSCV were generated and cultured as previously described (22). BJ cells expressing human telomerase (hTERT), SV40 large T (LT) and mutant $HRAS^{G12V}$ (hTERT/LT/$HRAS^{G12V}$) and control hTERT/LT were a kind gift from William C. Hahn (Dana-Farber Cancer Institute, Boston, U. S. A). H460 cells were a kind gift from Julian Downward (Francis Crick Institute, London, UK). MIA PaCa-2 cells were a kind gift from Barbara Grüner (German Cancer Consortium DKTK, Essen, Germany). HEK293T and CFPAC1 cells were purchased from American Type Culture Collection (Rockville, MD). Unless otherwise specified, all cell lines were maintained in DMEM (Gibco) supplemented with 10% fetal calf serum (FCS; Sigma Aldrich). All cells were kept at 37 °C with 5% CO2 and tested for mycoplasma at regular intervals.

Murine pancreatic tumor organoids treatment

Pancreatic tumor organoids were generated as previously described (23). Organoids were seeded at 100 cells/well, with or without SPRi3 (50 μM) treatment and allowed to grow for one week following which RSL3 (1 μM) treatments were added for an additional 48 hours. Organoid sizes were imaged and quantified using the BZ-H4M/Measurement Application Software (Keyence).

Full Materials and Methods available in Supplemental information

Acknowledgements

Research in the lab of G.L. was funded by the Deutsche Forschungsgemeinschaft (grant no. LE 3751/2-1), the German Cancer Aid (grant no. 70112624), the Elterninitiative Düsseldorf e.V. (grant no. 701910003), the Dr. Rolf M. Schwiete Stiftung (grant no. 2020-018) and the Research Commission of the Medical Faculty, Heinrich Heine University Düsseldorf (grant no. 2016-056 and 2020-044). J.K.M.L was supported by the Deutsche Forschungsgemeinschaft (Walter Benjamin Fellowship no. LI3844/1-1), the Dr. Rolf M. Schwiete Stiftung (grant no. 2023-029) and the Research Commission of the Medical Faculty, Heinrich Heine University Düsseldorf (grant no. 2022-12). Research in the lab of S.v.K was funded by: a collaborative research center grant on cell death (CRC1403, project ID 414786233), predictability in evolution (CRC1310, project ID 325931972), small cell lung cancer (CRC1399, project ID 413326622), B-cell lymphomas (CRC1530, project ID 455784452), through a priority program on ferroptosis (SPP2306, project ID 461704389) all funded by the Deutsche Forschungsgemeinschaft, an eMed consortium grant by the BMBF (InCa-01ZX1901A), via CANTAR which is funded through the program " Netzwerke 2021", an initiative of the Ministry of Culture and Science of the State of Northrhine Westphalia, Germany and a project grant (A06) funded by the center for molecular medicine cologne (CMMC). Research in the lab of F.B. was funded by the Deutsche Forschungsgemeinschaft (SFB1399 grant no. 41332662), the German Cancer Aid (grant no. 70113041) and the Mildred Scheel Nachwuchszentrum (grant no. 70113307). J.B. was funded by: a collaborative research center grant on small cell lung cancer (CRC1399 grant no. 413326622) by the Deutsche Forschungsgemeinschaft, via CANTAR which is funded through the program " Netzwerke 2021", an initiative of the Ministry of Culture and Science of the State of Northrhine Westphalia, Germany, a career advancement grant by the Center for Molecular Medicine Cologne (CMMC, CAP18) and the Mildred Scheel Nachwuchszentrum (grant no. 70113307). C.B. was funded by the Deutsche Forschungsgemeinschaft via GRK2578 (project ID 417677437).

Author contributions

Conceptualization, J.K.M.L. and G.L.; Methodology, J.K.M.L., F.S., T.L., L.T., D.P., S.T., H.Z., O.L., J.B., F.B.; Resources, T.R., M.R., C.B., S.v.K., G.R., B.R.; Writing – Original Draft, J.K.M.L and G.L.; Writing – Review & Editing, J.K.M.L., F.S., S.T., H.Z., T.R., F.B., S.v.K., G.R., B.R., and G.L.; Visualization, J.K.M.L. and G.L.; Supervision, J.K.M.L and G.L.; Funding Acquisition, J.K.M.L., B.R., G.R. and G.L.

Competing interests

J.B. has received a research grant by Bayer AG outside of the presented work. The other authors declare no potential competing interests.

References

1. S. J. Dixon, *et al.*, Ferroptosis: an iron-dependent form of nonapoptotic cell death. *Cell* **149**, 1060–1072 (2012).

2. S. J. Dixon, *et al.*, Pharmacological inhibition of cystine-glutamate exchange induces endoplasmic reticulum stress and ferroptosis. *Elife* **3**, e02523 (2014).

3. W. S. Yang, *et al.*, Regulation of ferroptotic cancer cell death by GPX4. *Cell* **156**, 317–331 (2014).

4. J. P. Friedmann Angeli, *et al.*, Inactivation of the ferroptosis regulator Gpx4 triggers acute renal failure in mice. *Nat Cell Biol* **16**, 1180–1191 (2014).

5. S. Doll, *et al.*, FSP1 is a glutathione-independent ferroptosis suppressor. *Nature* **575**, 693–698 (2019).

452 6. K. Bersuker, *et al.*, The CoQ oxidoreductase FSP1 acts parallel to GPX4 to inhibit
453 ferroptosis. *Nature* **575**, 688–692 (2019).

454 7. V. A. N. Kraft, *et al.*, GTP Cyclohydrolase 1/Tetrahydrobiopterin Counteract Ferroptosis
455 through Lipid Remodeling. *ACS Cent Sci* **6**, 41–53 (2020).

456 8. M. Soula, *et al.*, Metabolic determinants of cancer cell sensitivity to canonical ferroptosis
457 inducers. *Nat Chem Biol* **16**, 1351–1360 (2020).

458 9. H.-F. Zhang, R. I. Klein Geltink, S. J. Parker, P. H. Sorensen, Transsulfuration, minor
459 player or crucial for cysteine homeostasis in cancer. *Trends Cell Biol* **32**, 800–814
460 (2022).

461 10. L. Jiang, *et al.*, Ferroptosis as a p53-mediated activity during tumour suppression.
462 *Nature* **520**, 57–62 (2015).

463 11. Y. Zhang, *et al.*, BAP1 links metabolic regulation of ferroptosis to tumour suppression.
464 *Nat Cell Biol* **20**, 1181–1192 (2018).

465 12. S. Dolma, S. L. Lessnick, W. C. Hahn, B. R. Stockwell, Identification of genotype-
466 selective antitumor agents using synthetic lethal chemical screening in engineered
467 human tumor cells. *Cancer Cell* **3**, 285–296 (2003).

468 13. N. Yagoda, *et al.*, RAS-RAF-MEK-dependent oxidative cell death involving voltage-
469 dependent anion channels. *Nature* **447**, 864–868 (2007).

470 14. W. S. Yang, B. R. Stockwell, Synthetic lethal screening identifies compounds activating
471 iron-dependent, nonapoptotic cell death in oncogenic-RAS-harboring cancer cells. *Chem*
472 *Biol* **15**, 234–245 (2008).

473 15. I. Poursaitidis, *et al.*, Oncogene-Selective Sensitivity to Synchronous Cell Death
474 following Modulation of the Amino Acid Nutrient Cystine. *Cell Rep* **18**, 2547–2556
475 (2017).

476 16. J. L. Bos, ras oncogenes in human cancer: a review. *Cancer Res* **49**, 4682–4689 (1989).

477 17. J. Downward, Targeting RAS signalling pathways in cancer therapy. *Nat Rev Cancer* **3**,
478 11–22 (2003).

479 18. Y. Pylayeva-Gupta, E. Grabocka, D. Bar-Sagi, RAS oncogenes: weaving a tumorigenic
480 web. *Nat Rev Cancer* **11**, 761–774 (2011).

481 19. A. D. Cox, C. J. Der, The dark side of Ras: regulation of apoptosis. *Oncogene* **22**, 8999–
482 9006 (2003).

483 20. S. von Karstedt, *et al.*, Cancer cell-autonomous TRAIL-R signaling promotes KRAS-
484 driven cancer progression, invasion, and metastasis. *Cancer Cell* **27**, 561–573 (2015).

485 21. F. J. H. Hoogwater, *et al.*, Oncogenic K-Ras turns death receptors into metastasis-
486 promoting receptors in human and mouse colorectal cancer cells. *Gastroenterology* **138**,
487 2357–2367 (2010).

488 22. J. K. M. Lim, *et al.*, Cystine/glutamate antiporter xCT (SLC7A11) facilitates oncogenic
489 RAS transformation by preserving intracellular redox balance. *Proc Natl Acad Sci U S A*
490 **116**, 9433–9442 (2019).

491 23. F. Müller, *et al.*, Elevated FSP1 protects KRAS-mutated cells from ferroptosis during
492 tumor initiation. *Cell Death Differ* **30**, 442–456 (2023).

493 24. W. C. Hahn, *et al.*, Enumeration of the simian virus 40 early region elements necessary
494 for human cell transformation. *Mol Cell Biol* **22**, 2111–2123 (2002).

495 25. A. Tsherniak, *et al.*, Defining a Cancer Dependency Map. *Cell* **170**, 564-576.e16 (2017).

496 26. F. M. Behan, *et al.*, Prioritization of cancer therapeutic targets using CRISPR-Cas9
497 screens. *Nature* **568**, 511–516 (2019).

498 27. P. East, *et al.*, RAS oncogenic activity predicts response to chemotherapy and outcome
499 in lung adenocarcinoma. *Nat Commun* **13**, 5632 (2022).

500 28. H.-F. Zhang, *et al.*, Proteomic Screens for Suppressors of Anoikis Identify IL1RAP as a
501 Promising Surface Target in Ewing Sarcoma. *Cancer Discov* **11**, 2884–2903 (2021).

502 29. A. L. Kennedy, *et al.*, Activation of the PIK3CA/AKT pathway suppresses senescence
503 induced by an activated RAS oncogene to promote tumorigenesis. *Mol Cell* **42**, 36–49
504 (2011).

505 30. S. R. Hingorani, *et al.*, Preinvasive and invasive ductal pancreatic cancer and its early
506 detection in the mouse. *Cancer Cell* **4**, 437–450 (2003).

507 31. A. N. Tran, *et al.*, Reactive species balance via GTP cyclohydrolase I regulates
508 glioblastoma growth and tumor initiating cell maintenance. *Neuro Oncol* **20**, 1055–1067
509 (2018).

510 32. S. J. F. Cronin, *et al.*, Phenotypic drug screen uncovers the metabolic GCH1/BH4
511 pathway as key regulator of EGFR/KRAS-mediated neuropathic pain and lung cancer.
512 *Sci Transl Med* **14**, eabj1531 (2022).

513 33. Z. Wang, *et al.*, GTP Cyclohydrolase Drives Breast Cancer Development and Promotes
514 EMT in an Enzyme-Independent Manner. *Cancer Res* **83**, 3400–3413 (2023).

515 34. L. Badea, V. Herlea, S. O. Dima, T. Dumitrascu, I. Popescu, Combined gene expression
516 analysis of whole-tissue and microdissected pancreatic ductal adenocarcinoma identifies
517 genes specifically overexpressed in tumor epithelia. *Hepatogastroenterology* **55**, 2016–
518 2027 (2008).

519 35. R. Janky, *et al.*, Prognostic relevance of molecular subtypes and master regulators in
520 pancreatic ductal adenocarcinoma. *BMC Cancer* **16**, 632 (2016).

521 36. M. Ceccarelli, *et al.*, Molecular Profiling Reveals Biologically Discrete Subsets and
522 Pathways of Progression in Diffuse Glioma. *Cell* **164**, 550–563 (2016).

523 37. A. Méndez-Lucas, *et al.*, Identifying strategies to target the metabolic flexibility of
524 tumours. *Nat Metab* **2**, 335–350 (2020).

525 38. S. Cherradi, P. Martineau, C. Gongora, M. Del Rio, Claudin gene expression profiles and
526 clinical value in colorectal tumors classified according to their molecular subtype. *Cancer*
527 *Manag Res* **11**, 1337–1348 (2019).

528 39. A. L. Tarca, *et al.*, Strengths and limitations of microarray-based phenotype prediction:
529 lessons learned from the IMPROVER Diagnostic Signature Challenge. *Bioinformatics*
530 **29**, 2892–2899 (2013).

531 40. M. J. Hangauer, *et al.*, Drug-tolerant persister cancer cells are vulnerable to GPX4
532 inhibition. *Nature* **551**, 247–250 (2017).

533 41. V. S. Viswanathan, *et al.*, Dependency of a therapy-resistant state of cancer cells on a
534 lipid peroxidase pathway. *Nature* **547**, 453–457 (2017).

535 42. J. Tsoi, *et al.*, Multi-stage Differentiation Defines Melanoma Subtypes with Differential
536 Vulnerability to Drug-Induced Iron-Dependent Oxidative Stress. *Cancer Cell* **33**, 890-
537 904.e5 (2018).

538 43. R. P. Abrams, W. L. Carroll, K. A. Woerpel, Five-Membered Ring Peroxide Selectively
539 Initiates Ferroptosis in Cancer Cells. *ACS Chem Biol* **11**, 1305–1312 (2016).

540 44. J. K. M. Lim, G. Leprivier, The impact of oncogenic RAS on redox balance and
541 implications for cancer development. *Cell Death Dis* **10**, 955 (2019).

542 45. G. M. DeNicola, *et al.*, Oncogene-induced Nrf2 transcription promotes ROS
543 detoxification and tumorigenesis. *Nature* **475**, 106–109 (2011).

544 46. C. Schott, U. Graab, N. Cuvelier, H. Hahn, S. Fulda, Oncogenic RAS Mutants Confer
545 Resistance of RMS13 Rhabdomyosarcoma Cells to Oxidative Stress-Induced
546 Ferroptotic Cell Death. *Front Oncol* **5**, 131 (2015).

547 47. B. Thöny, G. Auerbach, N. Blau, Tetrahydrobiopterin biosynthesis, regeneration and
548 functions. *Biochem J* **347 Pt 1**, 1–16 (2000).

549 48. T. Homma, *et al.*, Nitric oxide protects against ferroptosis by aborting the lipid
550 peroxidation chain reaction. *Nitric Oxide* **115**, 34–43 (2021).

551 49. V. Bhatt, *et al.*, Inhibition of autophagy and MEK promotes ferroptosis in Lkb1-deficient
552 Kras-driven lung tumors. *Cell Death Dis* **14**, 61 (2023).

553 50. M. M. Awad, *et al.*, Acquired Resistance to KRASG12C Inhibition in Cancer. *N Engl J*
554 *Med* **384**, 2382–2393 (2021).

555 51. H. Thorvaldsdóttir, J. T. Robinson, J. P. Mesirov, Integrative Genomics Viewer (IGV):
556 high-performance genomics data visualization and exploration. *Brief Bioinform* **14**, 178–
557 192 (2013).

558

559 **Fig. 1.** Oncogenic activation of RAS signaling suppresses ferroptosis. (A) Cell death
560 quantification of NIH 3T3 cells expressing mutant $KRAS^{G12V}$ or control MSCV upon treatment
561 with ML162 (2 μM), ML210 (10 μM), FINO2 (20 μM), sulfasalazine (SSZ; 0.7 mM) or vehicle
562 for 24 h in the presence or absence of ferrostatin-1 (Fer-1; 5 μM), analyzed by propidium
563 iodide (PI) staining and flow cytometry. (B) Cell death quantification of BJ cells expressing
564 human telomerase (hTERT), SV40 large T (LT) and mutant $HRAS^{G12V}$ (hTERT/LT/$HRAS^{G12V}$)
565 or control hTERT/LT upon treatment with RSL3 (1 μM), ML162 (0.5 μM), ML210 (1 μM),
566 erastin (ERA; 5 μM) or vehicle for 24 h in the presence or absence of Fer-1 (5 μM), analyzed
567 as in (A). (C) Cell death quantification of shKRAS knockdown and scrambled (scr) control
568 CFPAC1 cells upon treatment with indicated concentrations of RSL3 for 24 h in the presence
569 or absence of Fer-1 (5 μM), analyzed as in (A) and (B). (D) Relative *KRAS* mRNA expression

570 in shKRAS knockdown and scr control CFPAC1 cells analyzed by qRT-PCR. (E) Correlation
571 between *KRAS* mutation status and sensitivity to ML162 in cancer cells. *wt, wild-type. mut,*
572 *mutant*. (F, G, H, and I) Correlation between *RAS* signature score and sensitivity to ML162,
573 RSL3, ML210, and erastin in cancer cells. RAS^{low} and RAS^{high} cells are divided according to
574 median AUC. (E-I) Data are obtained from the Cancer Therapeutic Response Portal v2
575 (CTRPv2) database, accessed via the DepMap portal. Higher AUC values indicate increased
576 resistance to compound treatment. Data represent mean ± SD of three independent
577 experiments. Unpaired, two-tailed *t test*; $^{*}P < 0.05$, $^{**}P < 0.01$, $^{***}P < 0.001$. ns, not significant.

578 **Fig. 2.** Oncogenic RAS signaling transcriptionally upregulates GCH1. (A) Volcano plots
579 comparing transcriptomic (RNA sequencing) and proteomic profiles of NIH 3T3 cells
580 expressing mutant $KRAS^{G12V}$ versus control MSCV. (B) Schematic depicting GCH1-mediated
581 tetrahydrobiopterin (BH4) biosynthesis. (C) Relative *Gch1* mRNA expression in NIH 3T3 cells
582 expressing mutant $KRAS^{G12V}$ and control MSCV analyzed by qRT-PCR. (D) Relative Gch1
583 peptide level in NIH 3T3 cells expressing mutant $KRAS^{G12V}$ and control MSCV analyzed by
584 mass spectrometry. (E) Relative *GCH1* mRNA expression in BJ cells expressing human
585 telomerase (hTERT), SV40 large T (LT) and mutant $HRAS^{G12V}$ (hTERT/LT/$HRAS^{G12V}$) or
586 control hTERT/LT analyzed by qRT-PCR. (F) Relative *GCH1* mRNA expression in shKRAS
587 knockdown and scrambled (scr) control CFPAC1 cells analyzed by qRT-PCR. (G) Relative
588 *GCH1* mRNA expression in shKRAS knockdown and scr control H460 cells analyzed by qRT-
589 PCR. (H) Relative *GCH1* mRNA expression analyzed by qRT-PCR and phosphorylated ERK
590 (p-ERK) levels analyzed by Western Blot, in MIA PaCa-2 cells upon treatment with AMG510
591 (10 μM) or vehicle for the indicated times. (I) Relative *GCH1* mRNA expression in IMR90 cells
592 expressing myristoylated AKT1 (myrAKT1), mutant $HRAS^{G12V}$, or control pBabe, analyzed by
593 microarray. Data are obtained from GSE45276, accessed via the R2 platform (http://r2.amc.nl)
594 (29). (J) Relative *Gch1* mRNA expression analyzed by qRT-PCR, and expression of indicated
595 proteins analyzed by Western Blot in NIH 3T3 cells expressing mutant $KRAS^{G12V}$ (NIH 3T3
596 $KRAS^{G12V}$) upon treatment with MEK inhibitor PD184352 (10 μM; MEKi), AKT inhibitor
597 MK2206 (10 μM; AKTi) or vehicle for the indicated times. Data represent mean ± SD of three
598 independent experiments. Unpaired, two-tailed *t test*; $^{*}P < 0.05$, $^{**}P < 0.01$, $^{***}P < 0.001$. ns,
599 not significant.

600 **Fig. 3.** GCH1 mediates oncogenic RAS-driven ferroptosis suppression in 2D models. (A) Cell
601 death quantification of NIH 3T3 cells expressing mutant $KRAS^{G12V}$ or control MSCV upon
602 treatment with indicated concentrations of erastin (Era) or vehicle for 24 h in the presence or
603 absence of dihydrobiopterin (BH2; 50 μM), tetrahydrobiopterin (BH4; 50 μM), or ferrostatin-1
604 (Fer-1; 5 μM), analyzed by propidium iodide (PI) staining and flow cytometry. (B) Cell death
605 quantification of NIH 3T3 cells expressing mutant $KRAS^{G12V}$ or control MSCV upon treatment
606 with indicated concentrations of FINO2 or vehicle for 24 h in the presence or absence of BH2
607 (50 μM), BH4 (50 μM), or Fer-1 (5 μM), analyzed as in (A). (C) Lipid peroxidation quantification
608 of NIH 3T3 cells expressing mutant $KRAS^{G12V}$ or control MSCV upon treatment with indicated
609 concentrations of Era or vehicle for 6 h in the presence or absence of BH2 (50 μM), BH4 (50
610 μM), or Fer-1 (5 μM), analyzed by C11-BODIPY(581/591) staining and flow cytometry. (D)
611 Lipid peroxidation quantification of NIH 3T3 cells expressing mutant $KRAS^{G12V}$ or control
612 MSCV upon treatment with indicated concentrations of FINO2 or vehicle for 6 h in the
613 presence or absence of dihydrobiopterin BH2 (50 μM), BH4 (50 μM), or Fer-1 (5 μM), analyzed
614 as in (C). (E) Cell death quantification of shKRAS knockdown CFPAC1 cells upon treatment
615 with RSL3 (5 μM) for 24 h in the presence or absence of BH2 (50 μM) or BH4 (50 μM),
616 analyzed as in (A) and (B). (F) Relative *Gch1* mRNA expression in CRISPR interference
617 (CRISPRi)-mediated Gch1 knockdown (sgGch1-1 and sgGch1-2) and EGFP knockdown
618 (sgEGFP) control NIH 3T3 cells expressing mutant $KRAS^{G12V}$ (NIH 3T3 $KRAS^{G12V}$), analyzed
619 by qRT-PCR. (G) Cell death quantification of sgGch1-1, sgGch1-2, and sgEGFP NIH 3T3
620 $KRAS^{G12V}$ cells upon treatment with indicated concentrations of Era or vehicle for 24 h in the
621 presence or absence of BH2 (50 μM) or BH4 (50 μM), or Fer-1 (5 μM), analyzed as in (A) and

(B). Data represent mean ± SD of three independent experiments. Unpaired, one-tailed *t test*; *$P < 0.05$, **$P < 0.01$, ***$P < 0.001$. ns, not significant.

Fig. 4. GCH1 mediates oncogenic RAS-driven ferroptosis suppression in 3D models. (A) Colony formation of CRISPR interference (CRISPRi)-mediated Gch1 knockdown (sgGch1-1 and sgGch1-2) and control (sgEGFP) NIH 3T3 cells expressing mutant $KRAS^{G12V}$ (NIH 3T3 $KRAS^{G12V}$) grown in soft agar for 21 days and treated with the indicated concentrations of RSL3. Colonies were imaged and quantified using ImageJ, and normalized to control. (B) Colony formation of NIH 3T3 $KRAS^{G12V}$ cells grown in soft agar for 21 days and treated with SPRi3 or RSL3, alone or in combination. Colonies were imaged and quantified using ImageJ, and normalized to control. (C) Pancreatic organoids were seeded with or without SPRi3 (50 μM) and allowed to grow for one week following which RSL3 (1 μM) treatments were added for 48 hours. Organoids were imaged and quantified using the BZ-H4M/Measurement Application Software (Keyence). Data represent mean ± SD of three independent experiments. Unpaired, one-tailed *t test*; *$P < 0.05$, **$P < 0.01$, ***$P < 0.001$. ns, not significant.

Fig. 5. GCH1 expression is clinically relevant and correlates with oncogenic RAS activation in human cancers. (A) Pan-cancer analysis of *GCH1* expression in tumor samples stratified according to *KRAS* mutation status. *wt, wild-type. mut, mutant*. Data are obtained from The Cancer Genome Atlas (TCGA), analyzed using the cBioPortal platform. (B, C, and D) *GCH1* expression in tumor samples of pancreatic adenocarcinoma (PAAD), colon adenocarcinoma (COAD), and lung adenocarcinoma (LUAD) from TCGA, in comparison to corresponding non-tumor tissue from TCGA and/or Genotype-Tissue Expression (GTEx) database. Data are analyzed using the UCSC Xena portal. (E, F, G, H, I, and J) Correlation of *GCH1* expression and *RAS* signature score in tumor samples of COAD, rectal adenocarcinoma (READ), uterine carcinosarcoma (UCS), skin cutaneous melanoma (SKCM), low-grade glioma (LGG), and glioblastoma (GBM). Data are obtained from TCGA, accessed via the DepMap portal. Correlations were quantified using Spearman's rank correlation coefficient. (K) Over-representation analysis for Human Molecular Signatures Database (MSigDB) Hallmark gene sets of genes positively co-expressed with *GCH1* in tumor samples of GBM from TCGA, analyzed using the R2 platform. (L) *Gch1* expression in tumor samples from a mouse model of high-grade glioma with *p53fl/fl;Nf1fl/fl* driven by Ascl1 Cre-ERTM, in comparison to non-tumor tissue, obtained from GSE57036, accessed via the R2 platform. Data represent mean ± SD of three independent experiments. Unpaired, two-tailed *t test*; *$P < 0.05$, **$P < 0.01$, ***$P < 0.001$. ns, not significant.

Fig. 6. Transcriptional upregulation of GCH1 by oncogenic RAS signaling is mediated by ETS1. (A) Gene set enrichment analysis (GSEA) of NIH 3T3 cells expressing mutant $KRAS^{G12V}$ (NIH 3T3 $KRAS^{G12V}$) versus control MSCV showing enrichment for ETS1-regulated genes. (B) Schematic depicting regulation of ETS1 downstream of RAS-MAPK signaling pathway. (C) Relative *Gch1* mRNA expression analyzed by qRT-PCR and Ets-1 levels analyzed by Western Blot in siRNA-mediated Ets-1 knockdown (siEts-1) and scrambled (siScr) control NIH 3T3 $KRAS^{G12V}$ cells. (D) Relative *GCH1* mRNA expression analyzed by qRT-PCR and ETS1 levels analyzed by Western Blot in si-ETS1 knockdown (siETS1-1 and siETS1-2) and siScr control H460 cells. (E) Schematic depicting the transcriptionally active region (TAR) of *GCH1* and ETS1 binding sites. (F) Activity measurements of a reporter construct consisting of the TAR of *GCH1* directly upstream of *Firefly luciferase* (FLuc; *GCH1-Luc*), normalized to control *Renilla luciferase* (RLuc), upon co-expression with the indicated amounts of *ETS1*-expressing plasmid in HEK293T cells, and ETS1 expression levels analyzed by Western Blot. *A. U., Arbitrary units*. (G) Activity measurements of *GCH1-Luc* or *GCH1-Luc* with mutations in individual *ETS1* binding sites (*$GCH1^{mut}$-Luc*-1, 2, or 3) or all ETS1 binding sites (*$GCH1^{mut}$-Luc*-all) normalized to RLuc, upon co-expression with 400 ng of *ETS1*-expressing plasmid in HEK293T cells, and ETS1 expression levels analyzed by Western Blot. (H) ChIP-qPCR analysis showing occupancy of Ets-1 at the *Gch1* locus in NIH 3T3 $KRAS^{G12V}$ cells. (I) ChIP-sequencing data showing ETS1, H3K4me3, and H3K27ac occupancy profiles at the *GCH1* locus, in HepG2 cells. Data are obtained from UCSC Encode database, analyzed

using Integrative Genomics Viewer (IGV) (51). (J) Correlation between *GCH1* expression and ETS1 protein levels across multiple tumor entities from the Clinical Proteomic Tumor Analysis Consortium (CPTAC) and TCGA, analyzed using the cBioPortal platform. (K, L, and M) Correlation of *GCH1* expression and *ETS1* expression in tumor samples of PAAD, COAD, and lung adenocarcinoma (LUAD) obtained from GSE62165, GSE72970, and GSE43580 respectively, accessed via the R2 platform (35, 38, 39). Correlations were quantified using Spearman's rank correlation coefficient. Data represent mean ± SD of three independent experiments. Unpaired, two-tailed *t test*; $^{*}P < 0.05$, $^{**}P < 0.01$, $^{***}P < 0.001$. ns, not significant.

Fig. S1. (A) Cell death quantification of NIH 3T3 cells expressing mutant $KRAS^{G12V}$ or control MSCV upon treatment with the indicated concentrations of erastin (Era) or vehicle for 24 h in the presence or absence of ferrostatin-1 (Fer-1; 5 μM), analyzed by propidium iodide (PI) staining and flow cytometry. (B and C) Relative *GCH1* and *xCT* mRNA expression in BJ cells expressing human telomerase (hTERT), SV40 large T (LT) and mutant $HRAS^{G12V}$ (hTERT/LT/$HRAS^{G12V}$) or control hTERT/LT analyzed by qRT-PCR. Data represent the mean ± SEM. (D, E, and F) Correlation between *KRAS* mutation status and sensitivity to RSL3, ML210, and erastin in cancer cells. *wt, wild-type. mut, mutant*. Data are obtained from the CTRP database, accessed via the DepMap portal. Data represent mean ± SD of three independent experiments. Unpaired, two-tailed *t test*; $^{*}P < 0.05$, $^{**}P < 0.01$, $^{***}P < 0.001$. ns, not significant.

Fig. S2. (A) *left,* Venn diagram depicting significantly altered transcripts and proteins (fold change > 2 or < -2; $p < 0.05$) in NIH 3T3 cells expressing mutant $KRAS^{G12V}$ relative to control MSCV based on RNA sequencing and proteomic profiling. *right*, Heatmap showing concordance in transcript and protein levels of 193 overlapping transcripts/proteins significantly altered in $KRAS^{G12V}$-expressing cells. (B) Relative *KRAS* mRNA expression in shKRAS knockdown and scrambled (scr) control H460 cells analyzed by qRT-PCR. (C) Relative *Gch1* mRNA expression in NIH 3T3 cells expressing mutant $KRAS^{G12V}$ (NIH 3T3 $KRAS^{G12V}$) upon treatment with MEK inhibitor PD184352 (10 μM; MEKi) or vehicle for the indicated times, analyzed by qRT-PCR. Data represent mean ± SD of three independent experiments. Unpaired, two-tailed *t test*; $^{*}P < 0.05$, $^{**}P < 0.01$, $^{***}P < 0.001$. ns, not significant.

Fig. S3. (A) Cell death quantification of sgGch1-1, sgGch1-2, and sgEGFP NIH 3T3 $KRAS^{G12V}$ cells upon treatment with indicated concentrations of FINO2 or vehicle for 24 h in the presence or absence of dihydrobiopterin (BH2; 50 μM) or tetrahydrobiopterin (BH4; 50 μM), or ferrostatin-1 (Fer-1; 5 μM), analyzed by propidium iodide (PI) staining and flow cytometry. (B) Ranking of correlation scores between GCH1 expression and sensitivity to CTRP compounds (median AUC). Data are obtained from the Cancer Therapeutic Response Portal v2 (CTRPv2) database, accessed via the DepMap portal. (C) Colony formation of CRISPR interference (CRISPRi)-mediated Gch1 knockdown (sgGch1-1 and sgGch1-2) and control (sgEGFP) NIH 3T3 cells expressing mutant $KRAS^{G12V}$ (NIH 3T3 $KRAS^{G12V}$) grown in soft agar for 21 days. Colonies were imaged and quantified using ImageJ, and normalized to control. Data represent mean ± SD of three independent experiments. Unpaired, one-tailed *t test*; $^{*}P < 0.05$, $^{**}P < 0.01$, $^{***}P < 0.001$. ns, not significant.

Fig. S4. (A and B) *GCH1* expression in tumor samples of PAAD in comparison to non-tumor tissue, obtained from GSE15471 and GSE62165, accessed via the R2 platform (34, 35) (C) *Gch1* expression in tumor samples from a mouse model of liver cancer driven by human c-MYC overexpression, in comparison to non-tumor tissue, obtained from GSE129013, accessed via the NCBI Gene Expression Omnibus (GEO) platform (37). Data represent mean ± SD of three independent experiments. Unpaired, two-tailed *t test*; $^{*}P < 0.05$, $^{**}P < 0.01$, $^{***}P < 0.001$. ns, not significant.

Fig. S5. (A) Gene set enrichment analysis (GSEA) of NIH 3T3 cells expressing mutant $KRAS^{G12V}$ (NIH 3T3 $KRAS^{G12V}$) versus control MSCV showing enrichment for target genes regulated by indicated transcription factors. (B) Correlation of *GCH1* expression and *ETS1* expression in tumor samples of pancreatic adenocarcinoma (PAAD) obtained from GSE15471

accessed via the R2 platform (34). Correlations were quantified using Spearman's rank correlation coefficient. Data represent mean ± SD of three independent experiments. Unpaired, two-tailed *t test*; $^{*}P < 0.05$, $^{**}P < 0.01$, $^{***}P < 0.001$. ns, not significant.

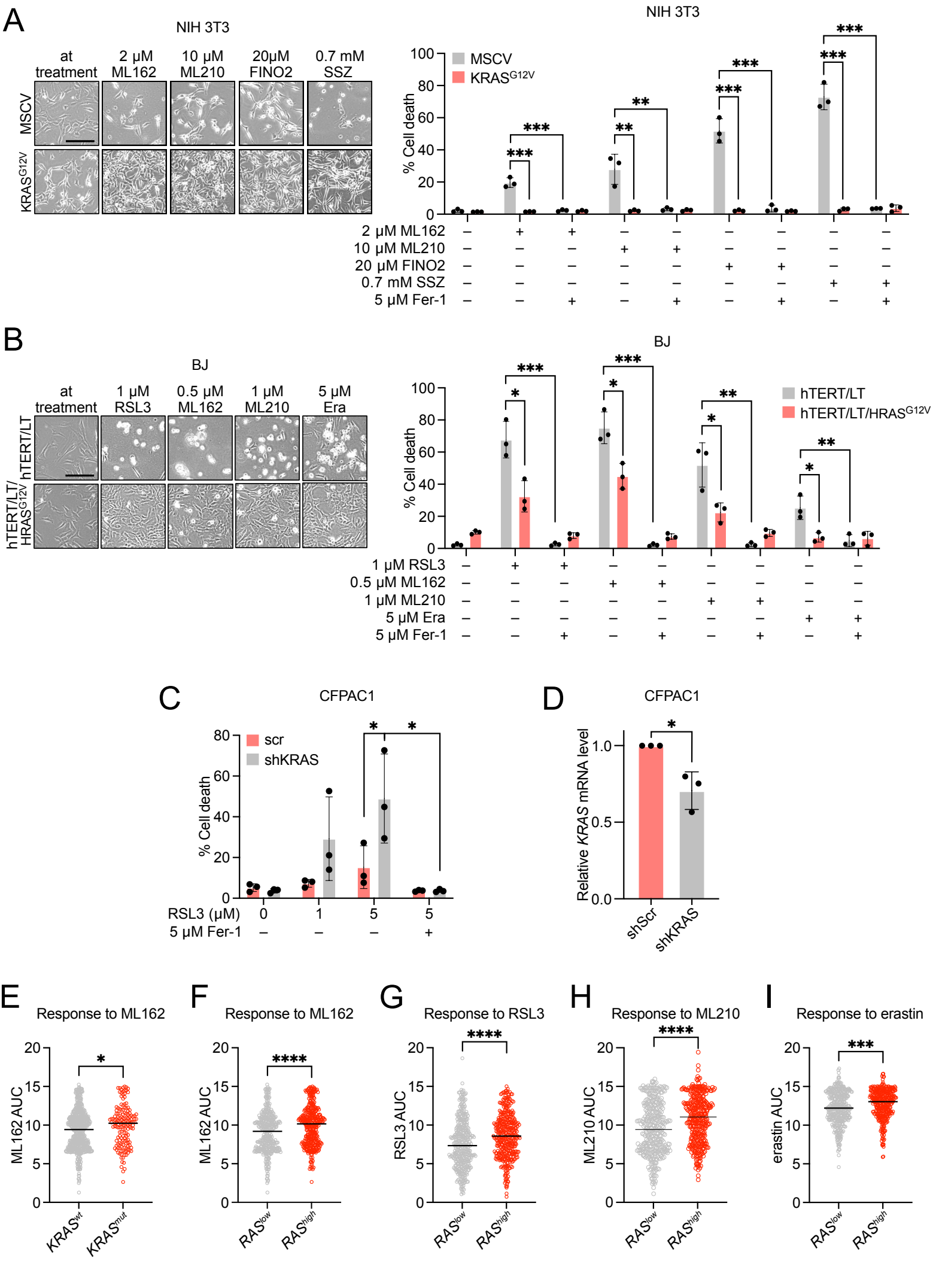
A
NIH 3T3
at treatment
2 μM ML162
10 μM ML210
20μM FINO2
0.7 mM SSZ
MSCV
KRASG12V
NIH 3T3
MSCV
KRASG12V
% Cell death
2 μM ML162
10 μM ML210
20 μM FINO2
0.7 mM SSZ
5 μM Fer-1
B
BJ
at treatment
1 μM RSL3
0.5 μM ML162
1 μM ML210
5 μM Era
hTERT/LT
hTERT/LT/HRASG12V
BJ
hTERT/LT
hTERT/LT/HRASG12V
% Cell death
1 μM RSL3
0.5 μM ML162
1 μM ML210
5 μM Era
5 μM Fer-1
C
CFPAC1
scr
shKRAS
% Cell death
RSL3 (μM)
5 μM Fer-1
D
CFPAC1
Relative KRAS mRNA level
shScr
shKRAS
E
Response to ML162
ML162 AUC
KRASwt
KRASmut
F
Response to ML162
ML162 AUC
RASlow
RAShigh
G
Response to RSL3
RSL3 AUC
RASlow
RAShigh
H
Response to ML210
ML210 AUC
RASlow
RAShigh
I
Response to erastin
erastin AUC
RASlow
RAShigh

Figure 1

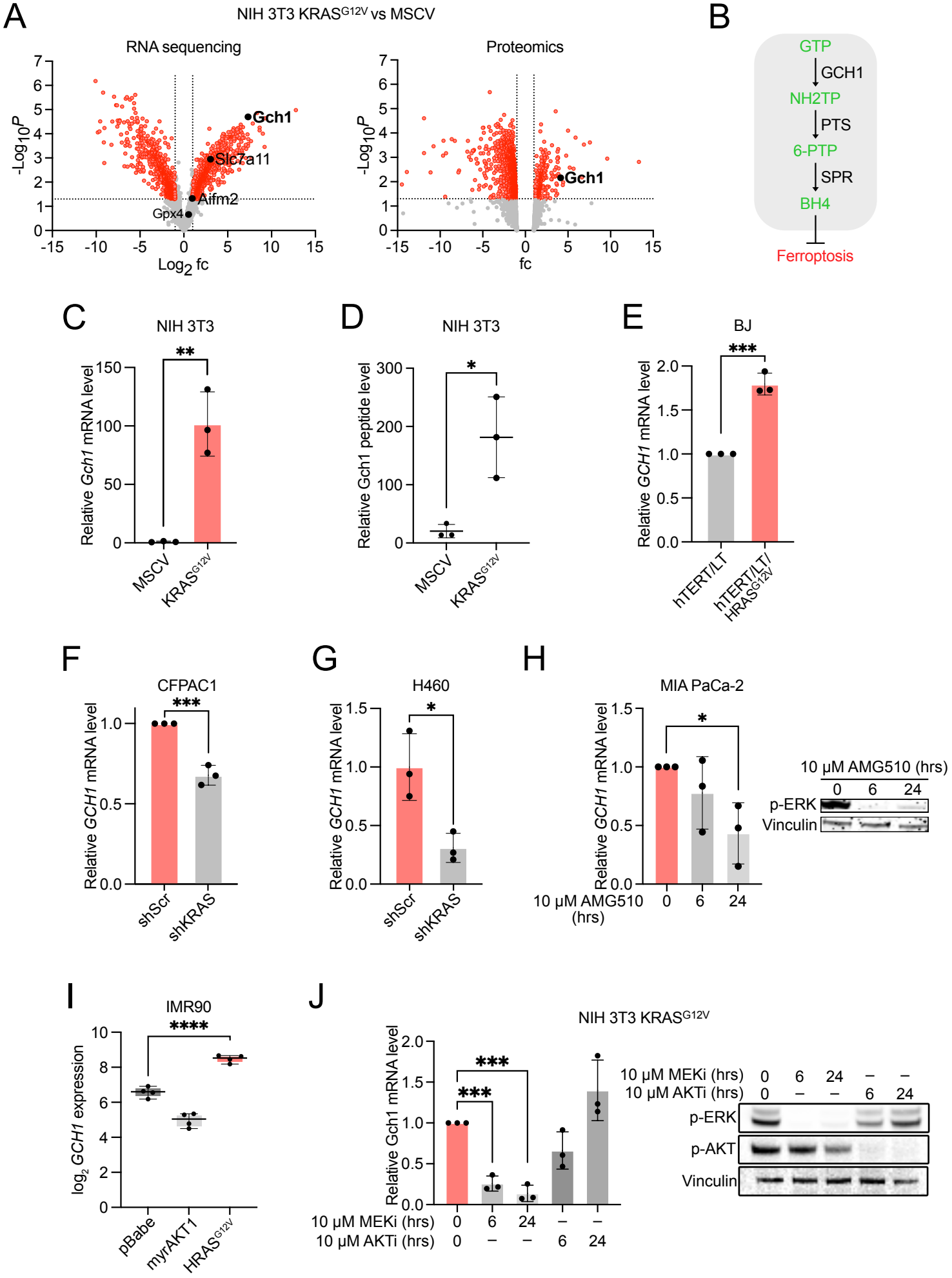
A
NIH 3T3 KRASG12V vs MSCV
RNA sequencing
Proteomics
-Log10P
Log2 fc
fc
Gch1
Slc7a11
Aifm2
Gpx4
B
GTP
GCH1
NH2TP
PTS
6-PTP
SPR
BH4
Ferroptosis
C
NIH 3T3
Relative Gch1 mRNA level
MSCV
KRASG12V
D
NIH 3T3
Relative Gch1 peptide level
E
BJ
Relative GCH1 mRNA level
hTERT/LT
hTERT/LT/ HRASG12V
F
CFPAC1
shScr
shKRAS
G
H460
H
MIA PaCa-2
10 μM AMG510 (hrs)
p-ERK
Vinculin
I
IMR90
log2 GCH1 expression
pBabe
myrAKT1
HRASG12V
J
NIH 3T3 KRASG12V
10 μM MEKi (hrs)
10 μM AKTi (hrs)
p-AKT

Figure 2

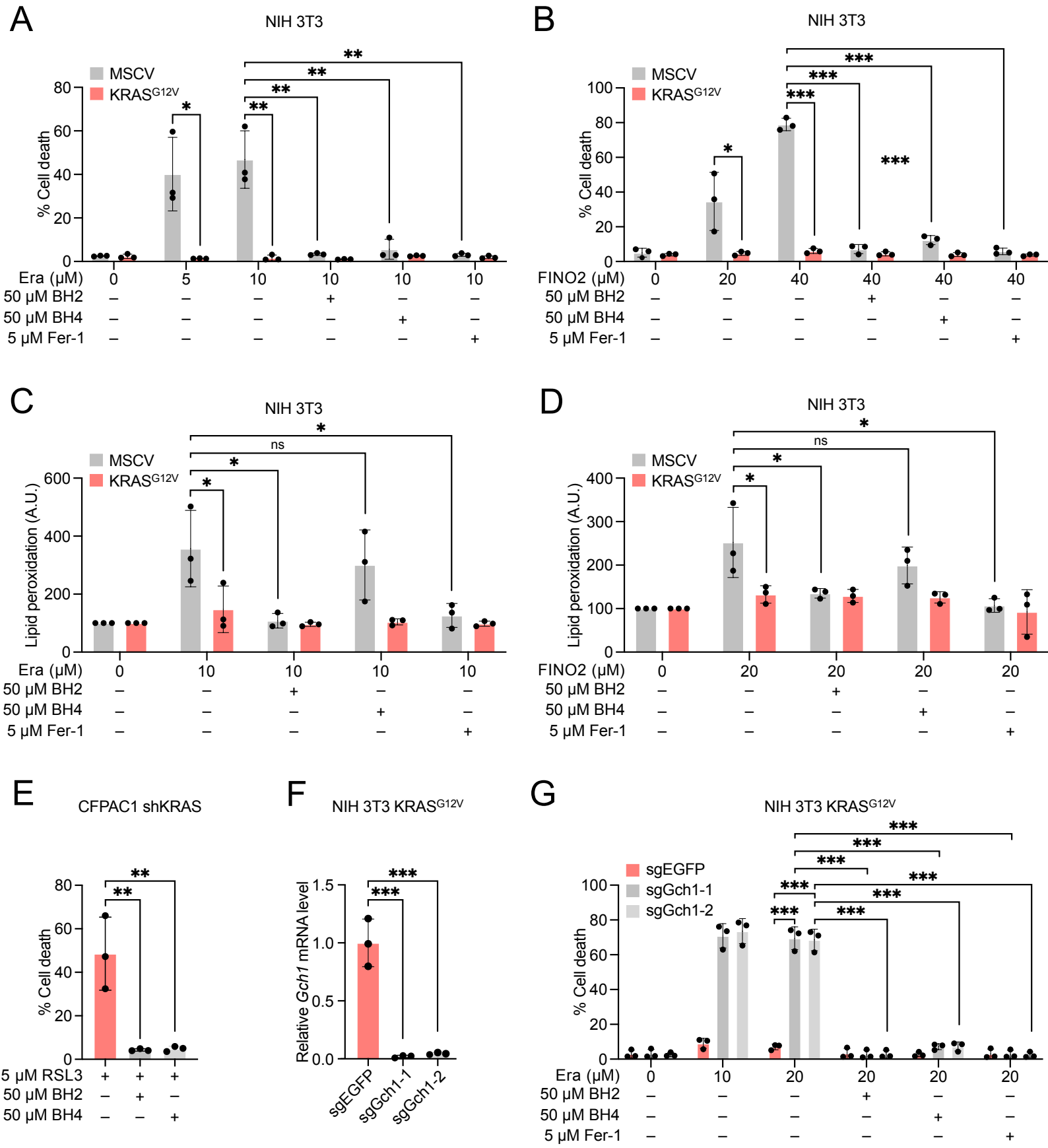
A
NIH 3T3
MSCV
KRASG12V
% Cell death
Era (μM) 0 5 10 10 10 10
50 μM BH2 – – – + – –
50 μM BH4 – – – – + –
5 μM Fer-1 – – – – – +
B
NIH 3T3
MSCV
KRASG12V
% Cell death
FINO2 (μM) 0 20 40 40 40 40
50 μM BH2 – – – + – –
50 μM BH4 – – – – + –
5 μM Fer-1 – – – – – +
C
NIH 3T3
MSCV
KRASG12V
Lipid peroxidation (A.U.)
Era (μM) 0 10 10 10 10
50 μM BH2 – – + – –
50 μM BH4 – – – + –
5 μM Fer-1 – – – – +
D
NIH 3T3
MSCV
KRASG12V
Lipid peroxidation (A.U.)
FINO2 (μM) 0 20 20 20 20
50 μM BH2 – – + – –
50 μM BH4 – – – + –
5 μM Fer-1 – – – – +
E
CFPAC1 shKRAS
% Cell death
5 μM RSL3 + + +
50 μM BH2 – + –
50 μM BH4 – – +
F
NIH 3T3 KRASG12V
Relative Gch1 mRNA level
sgEGFP
sgGch1-1
sgGch1-2
G
NIH 3T3 KRASG12V
sgEGFP
sgGch1-1
sgGch1-2
% Cell death
Era (μM) 0 10 20 20 20 20
50 μM BH2 – – – + – –
50 μM BH4 – – – – + –
5 μM Fer-1 – – – – – +

Figure 3

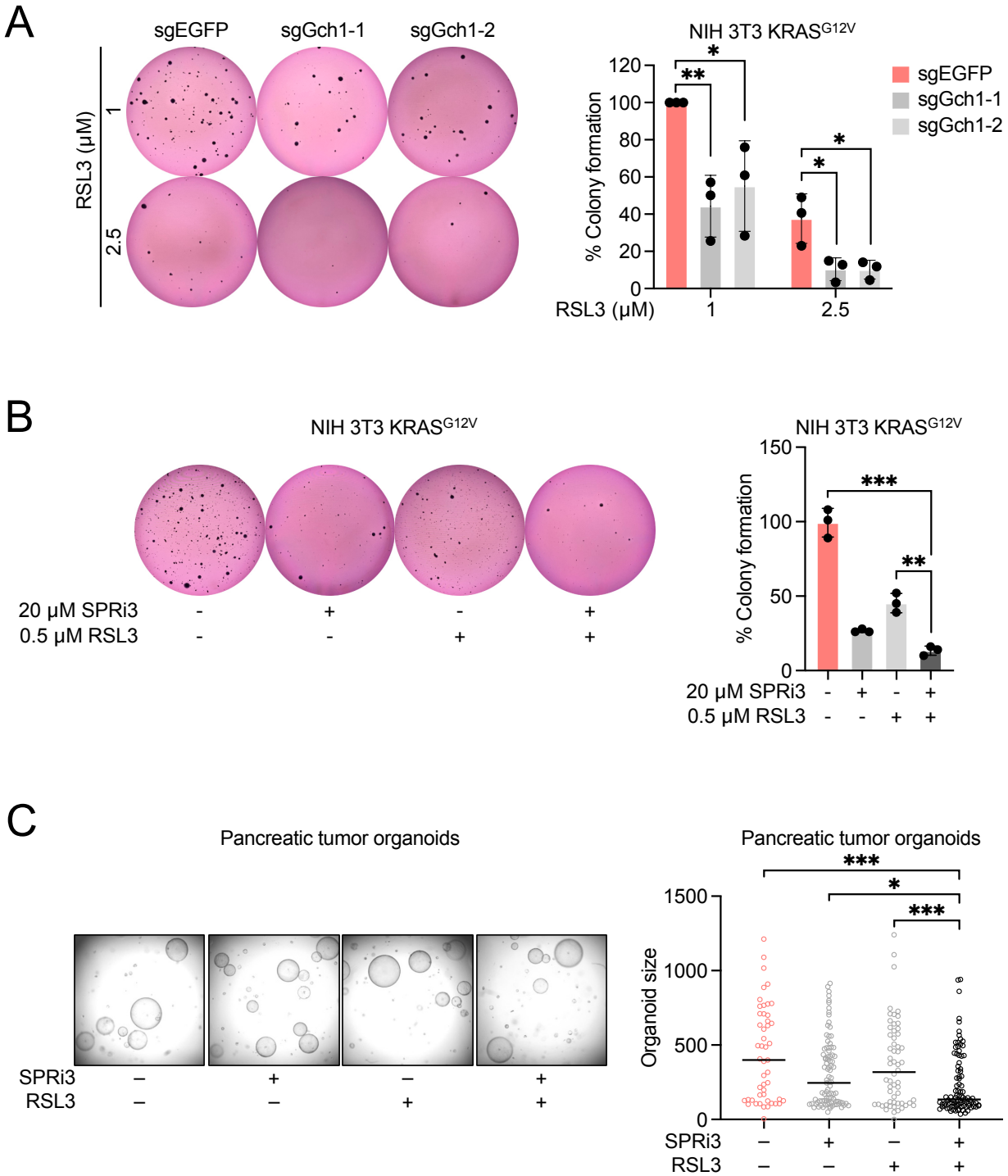
A
sgEGFP
sgGch1-1
sgGch1-2
RSL3 (μM)
1
2.5
NIH 3T3 KRAS^{G12V}
% Colony formation
120
100
80
60
40
20
0
*
**
*
*
sgEGFP
sgGch1-1
sgGch1-2
RSL3 (μM)
1
2.5
B
NIH 3T3 KRAS^{G12V}
20 μM SPRi3 - + - +
0.5 μM RSL3 - - + +
NIH 3T3 KRAS^{G12V}
% Colony formation
150
100
50
0
***
**
20 μM SPRi3 - + - +
0.5 μM RSL3 - - + +
C
Pancreatic tumor organoids
SPRi3 – + – +
RSL3 – – + +
Pancreatic tumor organoids
Organoid size
1500
1000
500
0
***
*
***
SPRi3 – + – +
RSL3 – – + +

Figure 4

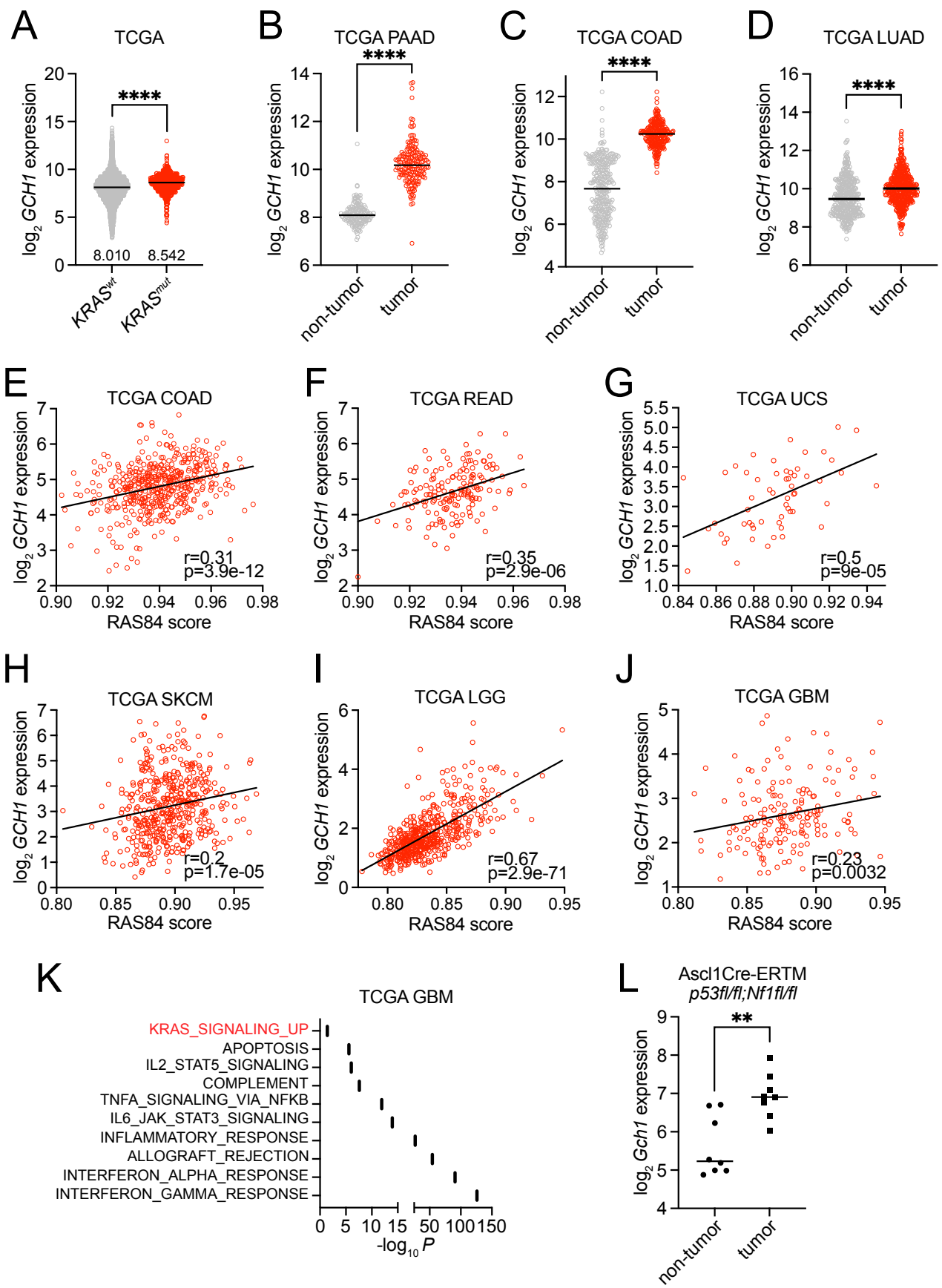
A
TCGA
****
log2 GCH1 expression
8.010
8.542
KRASwt
KRASmut
B
TCGA PAAD
****
non-tumor
tumor
C
TCGA COAD
****
D
TCGA LUAD
****
E
TCGA COAD
r=0.31
p=3.9e-12
RAS84 score
F
TCGA READ
r=0.35
p=2.9e-06
G
TCGA UCS
r=0.5
p=9e-05
H
TCGA SKCM
r=0.2
p=1.7e-05
I
TCGA LGG
r=0.67
p=2.9e-71
J
TCGA GBM
r=0.23
p=0.0032
K
TCGA GBM
KRAS_SIGNALING_UP
APOPTOSIS
IL2_STAT5_SIGNALING
COMPLEMENT
TNFA_SIGNALING_VIA_NFKB
IL6_JAK_STAT3_SIGNALING
INFLAMMATORY_RESPONSE
ALLOGRAFT_REJECTION
INTERFERON_ALPHA_RESPONSE
INTERFERON_GAMMA_RESPONSE
-log10 P
L
Ascl1Cre-ERTM
p53fl/fl;Nf1fl/fl
**
log2 Gch1 expression

Figure 5

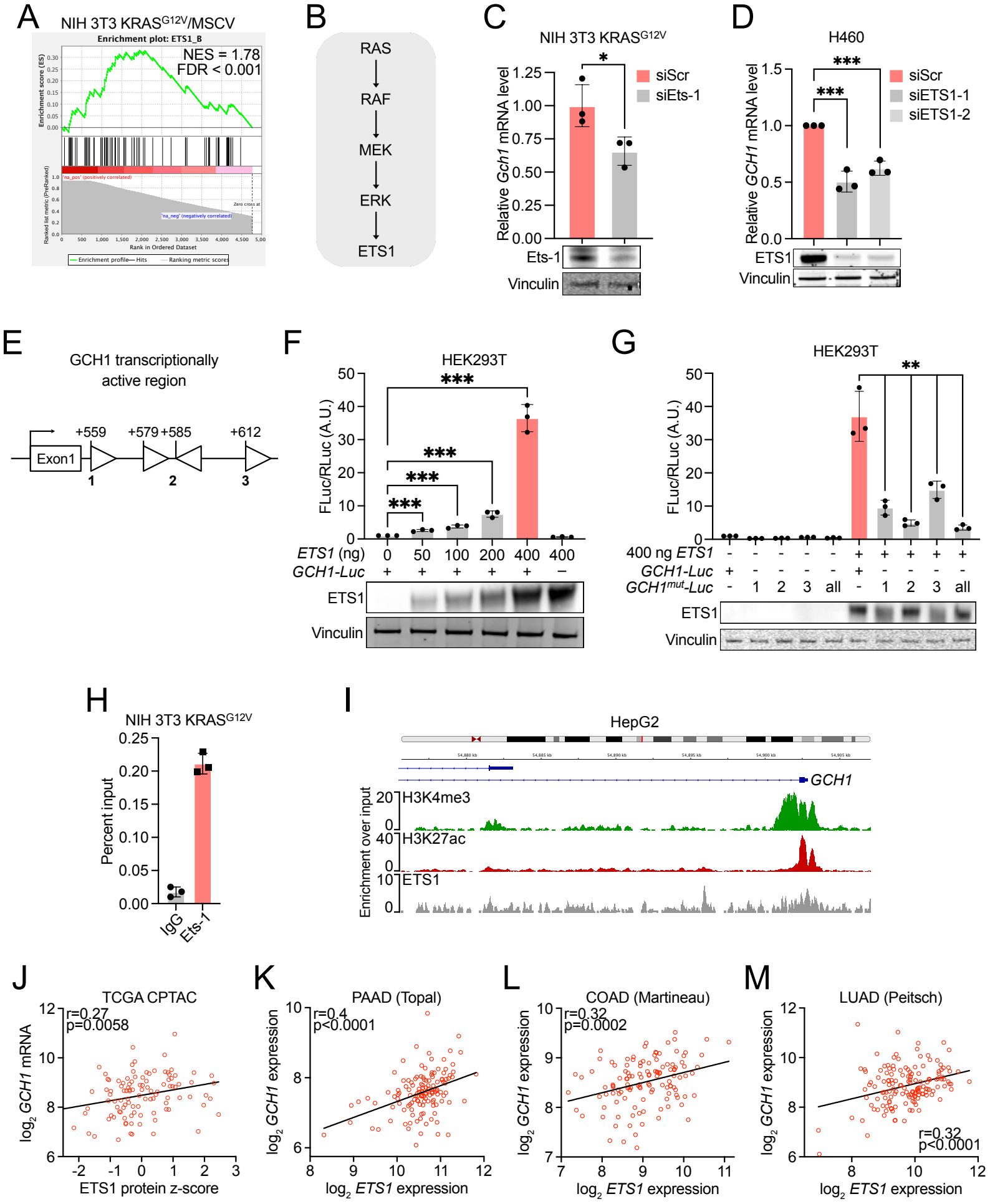
A
NIH 3T3 KRASG12V/MSCV
Enrichment plot: ETS1_B
NES = 1.78
FDR < 0.001
Rank in Ordered Dataset
B
RAS
RAF
MEK
ERK
ETS1
C
NIH 3T3 KRASG12V
Relative Gch1 mRNA level
siScr
siEts-1
Ets-1
Vinculin
D
H460
Relative GCH1 mRNA level
siScr
siETS1-1
siETS1-2
ETS1
Vinculin
E
GCH1 transcriptionally active region
Exon1
+559
+579 +585
+612
1
2
3
F
HEK293T
FLuc/RLuc (A.U.)
ETS1 (ng) 0 50 100 200 400 400
GCH1-Luc + + + + + –
ETS1
Vinculin
G
HEK293T
FLuc/RLuc (A.U.)
400 ng ETS1 - - - - - + + + + +
GCH1-Luc + - - - - + - - - -
GCH1mut-Luc - 1 2 3 all - 1 2 3 all
ETS1
Vinculin
H
NIH 3T3 KRASG12V
Percent input
IgG
Ets-1
I
HepG2
GCH1
H3K4me3
H3K27ac
ETS1
Enrichment over input
J
TCGA CPTAC
r=0.27
p=0.0058
log2 GCH1 mRNA
ETS1 protein z-score
K
PAAD (Topal)
r=0.4
p<0.0001
log2 GCH1 expression
log2 ETS1 expression
L
COAD (Martineau)
r=0.32
p=0.0002
log2 GCH1 expression
log2 ETS1 expression
M
LUAD (Peitsch)
r=0.32
p<0.0001
log2 GCH1 expression
log2 ETS1 expression

Figure 6

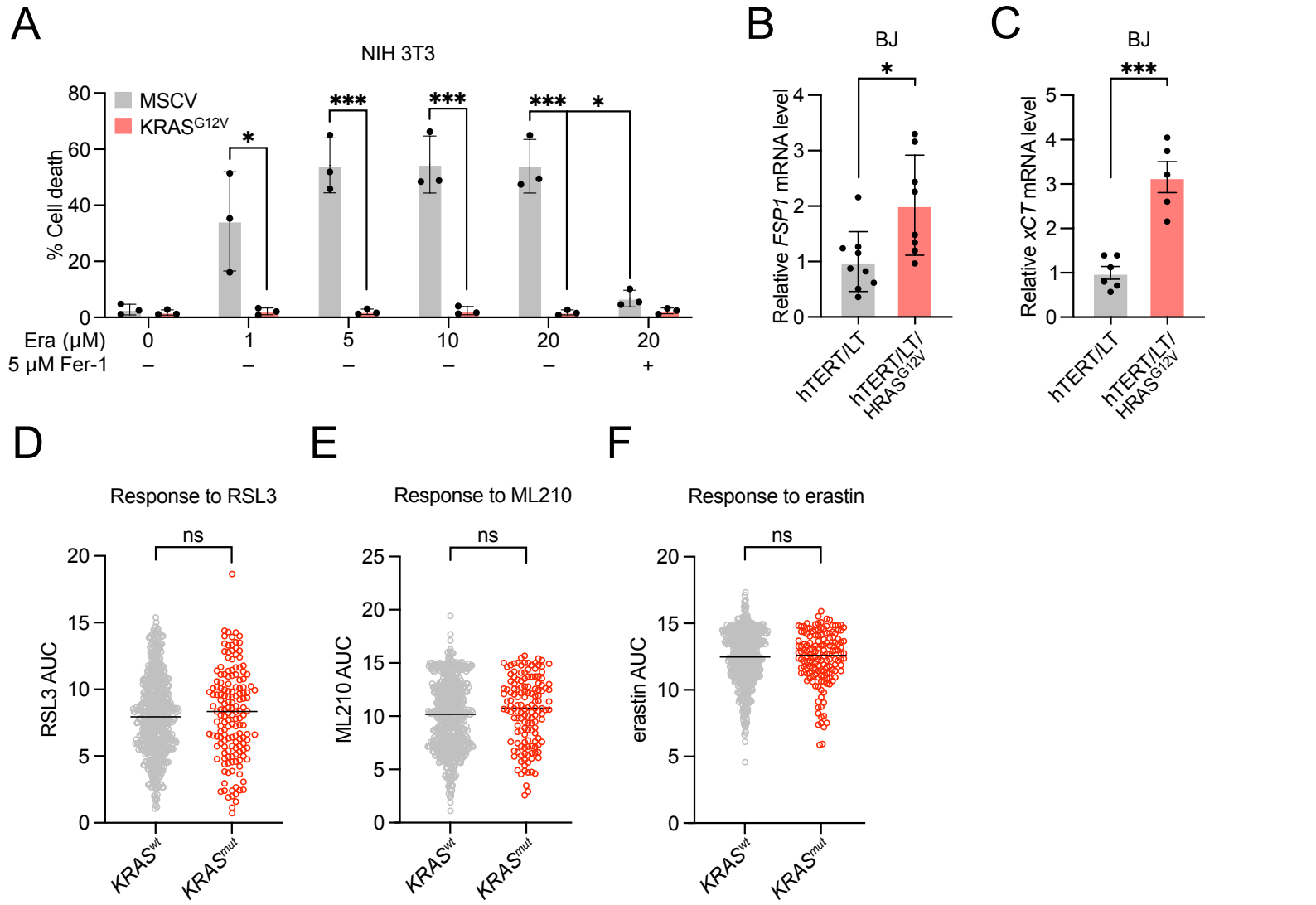

Supplementary Figure 1

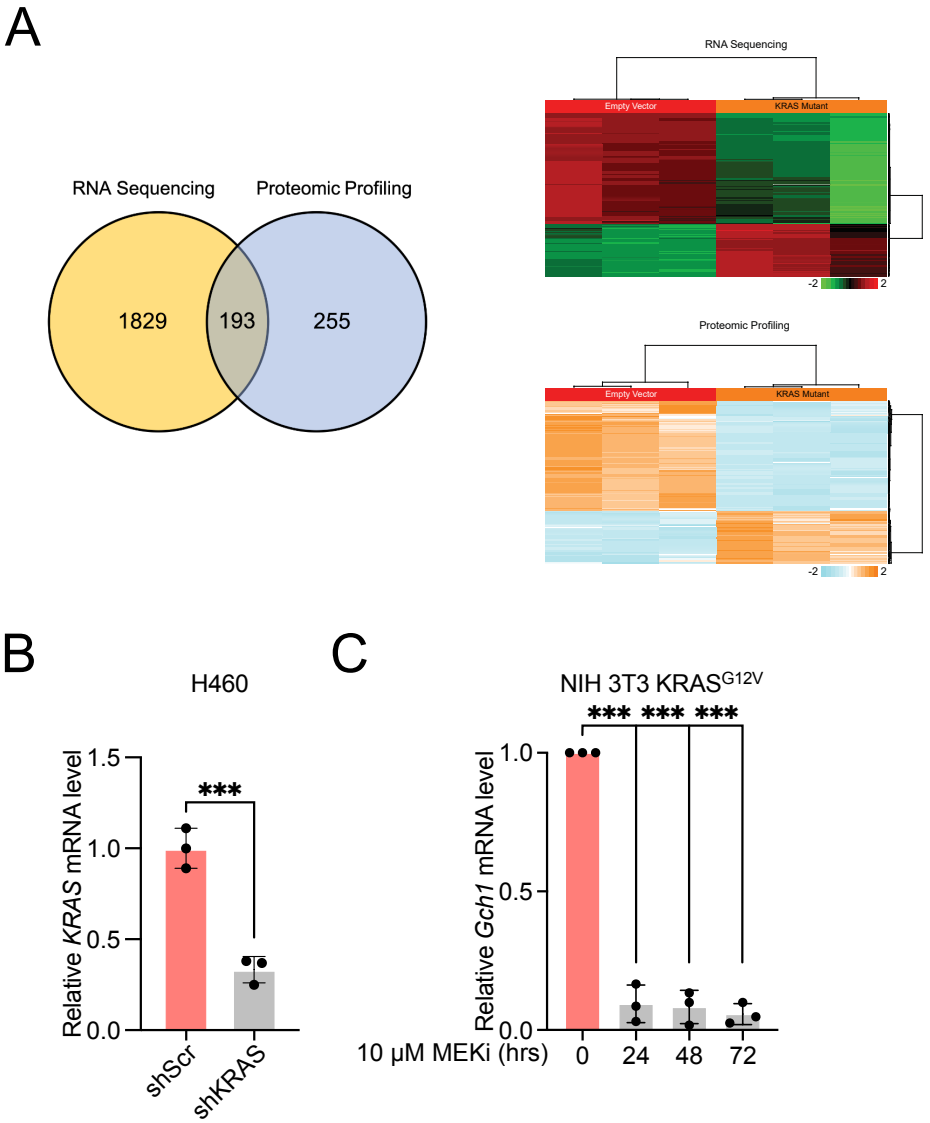

Supplementary Figure 2

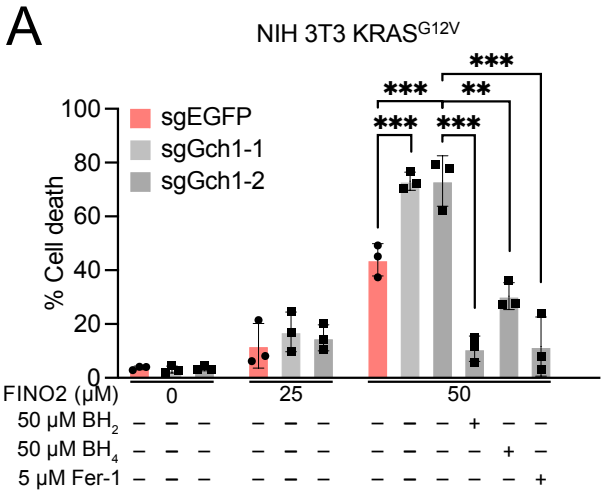

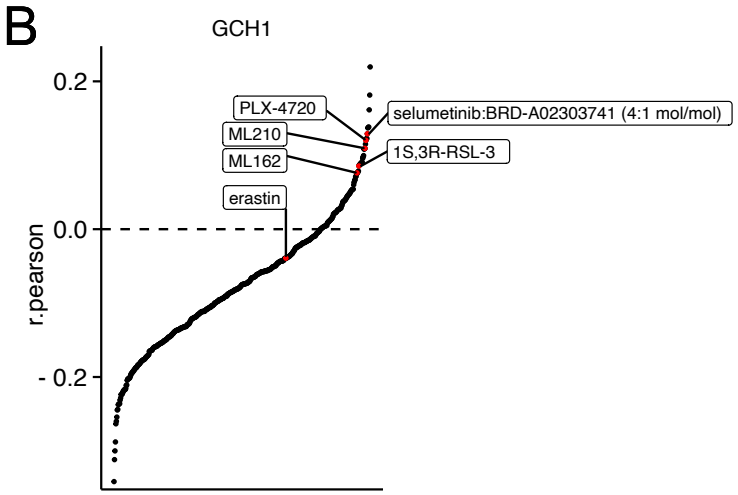

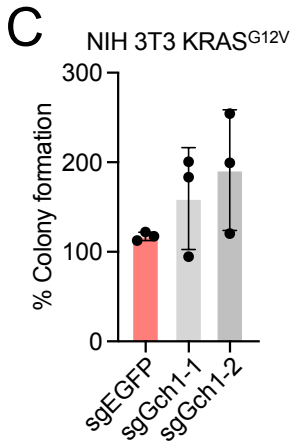

Supplementary Figure 3

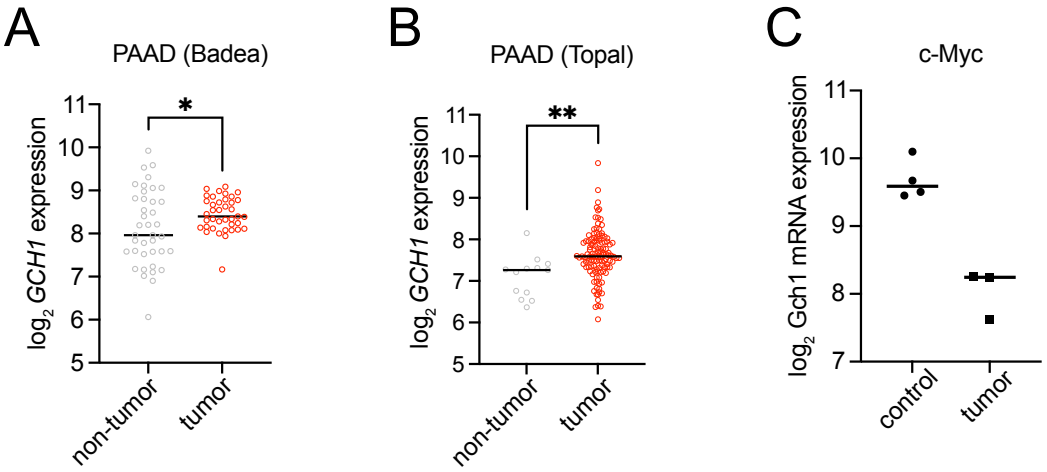

Supplementary Figure 4

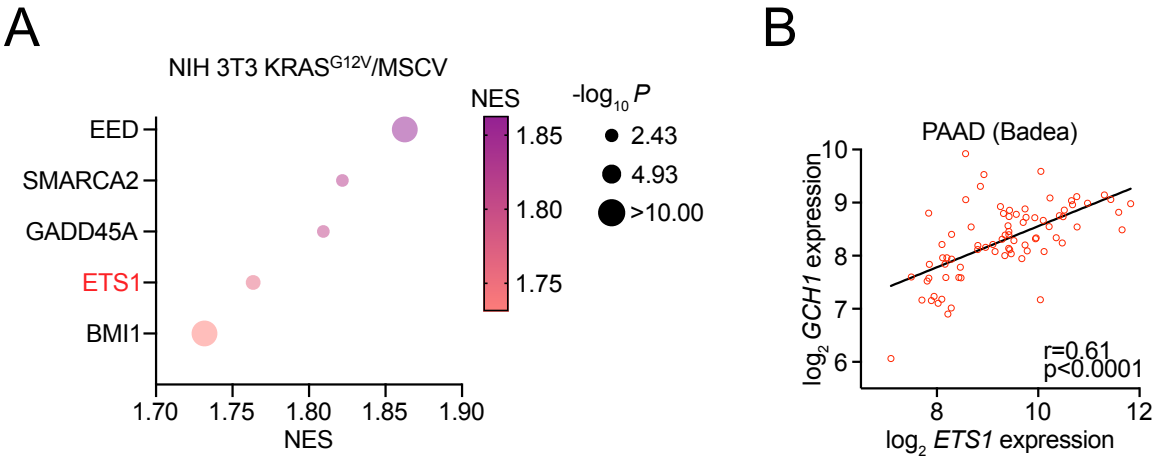

Supplementary Figure 5